Interplay between superconductivity and non-Fermi liquid at a quantum critical point in a metal. VI. The γ model and its phase diagram at $2 < \gamma < 3$

Shang-Shun Zhang,[1] Yi-Ming Wu,[1] Artem Abanov,[2] and Andrey V. Chubukov[1]
[1]*School of Physics and Astronomy and William I. Fine Theoretical Physics Institute, University of Minnesota, Minneapolis, Minnesota 55455, USA*
[2]*Department of Physics, Texas A&M University, College Station, Texas 77843, USA*

(Received 29 July 2021; revised 4 October 2021; accepted 5 October 2021; published 25 October 2021)

In this paper, the sixth in series, we continue our analysis of the interplay between non-Fermi liquid and pairing in the effective low-energy model of fermions with singular dynamical interaction $V(\Omega_m) = \bar{g}^\gamma/|\Omega_m|^\gamma$ (the γ model). The model describes low-energy physics of various quantum-critical metallic systems at the verge of an instability towards density or spin order, pairing of fermions at the half-filled Landau level, color superconductivity, and pairing in SYK-type models. In previous papers I–V, we analyzed the γ model for $\gamma \leqslant 2$ and argued that the ground state is an ordinary superconductor, but there is an infinite number of local minima of the condensation energy. We further argued that the condensation energy spectrum becomes continuous and gapless, and superconducting T_c vanishes due to critical longitudinal gap fluctuations. In this paper, we consider larger $2 < \gamma < 3$. We show that the system moves away from criticality in that the condensation energy spectrum again becomes discrete and gapless, and T_c becomes finite. Yet, we show that the gap functions for $\gamma > 2$ and $\gamma < 2$ are topologically different as they live on different sheets of the Riemann surface. This makes $\gamma = 2$ a topological quantum-critical point. We further show that the fermionic excitation spectrum for $\gamma > 2$ acquires a new feature—a bound state at the edge of a continuum, with a macroscopic degeneracy, which is a fraction of the total number of states in the system. We obtain the phase diagram on the (ω_D, γ) plane, where ω_D is a mass of a pairing boson, and on the (T, γ) plane. The latter consists of two distinct superconducting phases at $\gamma < 2$ and $\gamma > 2$ and the intermediate pseudogap state of preformed pairs in between.

DOI: 10.1103/PhysRevB.104.144509

I. INTRODUCTION

This paper continues our studies of the interplay between non-Fermi liquid (NFL) and superconductivity for itinerant fermions near a quantum-critical point (QCP) towards charge or spin order. The key interaction between fermions in this situation is mediated by soft bosonic order parameter fluctuations. When soft bosons are slow compared to electrons (e.g., when bosons are Landau-overdamped collective modes of fermions), the low-energy physics is described by an effective dynamical model with four-fermion interaction $V(\Omega) \propto 1/|\Omega|^\gamma$. At a QCP, when order parameter propagator is massless, this form holds down to $\Omega = 0$.

The model with $V(\Omega) \propto 1/|\Omega|^\gamma$ has been nicknamed the γ model. The exponent γ has particular values for a growing number of specific microscopic realizations: $\gamma = 0+$ for 3D quantum critical systems and for pairing of quarks, mediated by gluon exchange, $\gamma = 1/3$ for a system near a nematic QCP and for fermions at a half-filled Landau level, $\gamma = 1/2$ near an antiferromagnetic QCP, $\gamma = 0.68$ for Sachdev-Ye-Kitaev (SYK) model of N fermions coupled to equal number of bosons, $\gamma = 1$ for pairing by propagating bosons, $\gamma = 2$ for phonon-mediated pairing at vanishing Debye frequency, etc. Microscopic models with varying γ have also been proposed. We listed and discussed some microscopic models in the first paper of the series (paper I). In all cases, the same interaction, mediated by low-energy bosons, gives rise to fermionic self-energy, which accounts for NFL behavior in the normal state, and at the same time serves as the glue that binds fermions into pairs. The two tendencies (NFL and SC) are intertwined as they come from the same interaction, and compete with each other: a fermionic self-energy makes fermions incoherent and reduces the tendency to pairing, while if bound pairs develop, they provide a feedback on the self-energy, which at lowest frequencies recovers the Fermi liquid form, i.e., fermions become propagating rather than diffusive excitations.

For dispersion-full fermions SC emerges in a particular momentum channel, e.g., in a d-wave channel near an antiferromagnetic QCP. However, once the pairing symmetry is incorporated and momentum integration in the formulas for the fermionic self-energy and the pairing vertex is carried out, the effective low-energy model for different microscopic realizations becomes the same one, specified only by the value of γ. The sign of $V(\Omega)$ is attractive, i.e., if fermions were free, the ground state would necessarily be a superconductor.

In previous papers (Refs. [1–5]), which we refer to as papers I–V, we treated γ as a parameter and analyzed the interplay between NFL and pairing for $\gamma \leqslant 2$. In this paper we consider $2 < \gamma < 3$. For convenience of a reader, we list some results of previous works, which form the base for the analysis in this paper.

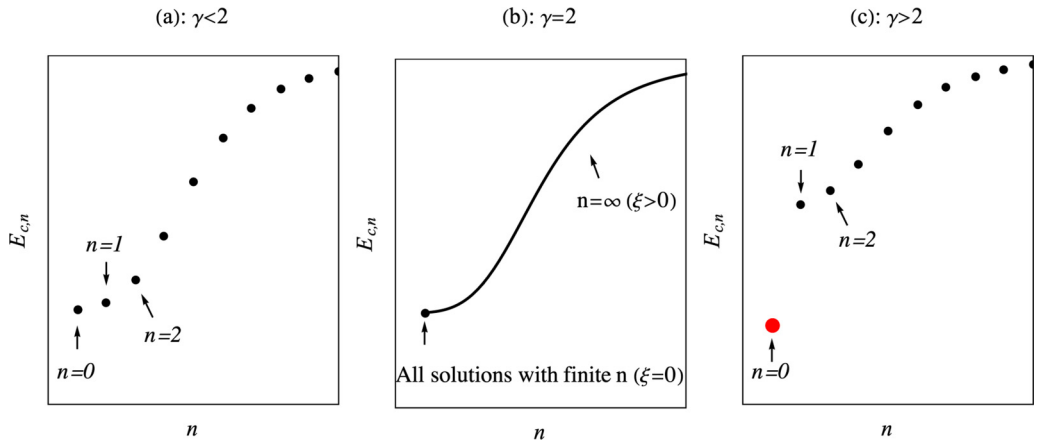

FIG. 1. The set of condensation energies $E_{c,n}$ for the solutions of the gap equation. For $\gamma < 2$ (a) and $\gamma > 2$ (c), the set is discrete and $|E_{c,0}|$ is the largest. For $\gamma = 2$ (b), the set is continuous: all $E_{c,n}$ with finite n coincide with $E_{c,0}$, while $E_{c,n}$ with $n = \infty$ form a continuous set.

(1) For any $0 \leqslant \gamma \leqslant 2$, the ground state is a superconductor, i.e., superconductivity wins the competition with a NFL. However, in distinction to the pairing of coherent fermions in a Fermi liquid, the pairing of incoherent fermions is a threshold phenomenon, and in an extended γ model with different magnitudes of $V(\Omega)$ in the particle-hole and particle-particle channels [$V(\Omega)$ and $V(\Omega)/N$, respectively], there exists a γ-dependent critical $N_{\rm cr} > 1$ separating a SC state for $N < N_{\rm cr}$ (including the original model with $N = 1$) and a NFL ground state for $N > N_{\rm cr}$.

(2) In another crucial distinction from pairing in a Fermi liquid, the gap equation at a QCP at $T = 0$ has an infinite set of solutions $\Delta_n(\omega)$, where n runs between 0 and ∞. At zero frequency, $\Delta_n(0) \propto e^{-An}$ are all finite (A is γ-dependent number). However, the $n-$ th solution changes sign n times along the Matsubara axis, $\omega \equiv \omega_m$. The solutions are then topologically distinct as each zero of $\Delta_n(\omega_m)$ is a center of a dynamical vortex on the upper complex plane of frequency. The $n = 0$ solution is sign-preserving and its structure along the Matsubara axis is similar to a conventional gap function in a Fermi liquid with attraction. The $n = \infty$ solution has an infinitesimally small magnitude and is the solution of the linearized gap equation. We presented the exact proof that the solution of the linearized gap equation exists along with the solutions of the nonlinear gap equation. Away from a QCP, only a finite number of solutions remain, and above a certain deviation from a QCP only the conventional $n = 0$ solution survives.

(3) Each solution from the infinite set at QCP evolves with T and vanishes at a separate $T_{p,n}$. The largest $T_{p,0} \sim \bar{g}$. At large n, $T_{p,n} \propto e^{-An}$. We presented strong numerical evidence for the existence of the set of critical temperatures and showed that the corresponding eigenfunctions change sign n times along the Matsubara axis.

(4) For $\gamma < 2$, the set is discrete, and the largest condensation energy at $T = 0$ and the highest pairing temperature T_p is for the $n = 0$ solution. In this respect, the ground state is still a "conventional" superconductor in the sense that $\Delta_0(\omega_m)$ is a regular, sign-preserving function of the Matsubara frequency. Phase fluctuations of $\Delta_0(\omega_m)$ are weak in the same parameter by which soft bosons are slow modes compared to fermions. However, as γ increases towards 2, the other solutions become progressively more relevant. Namely, the spectrum of the condensation energy $E_{c,n}$ becomes more dense and $E_{c,n}$ with $n > 0$ come closer to $E_{c,0}$. Simultaneously, the frequency range, where $\Delta_n(\omega_m)$ changes sign n times, shifts to progressively smaller $\omega_m \propto (2 - \gamma)$, while at larger frequencies all $\Delta_n(\omega_m)$ nearly coincide with $\Delta_0(\omega_m)$.

(5) At $\gamma = 2$, a critical behavior emerges: all $\Delta_n(\omega_m)$ with finite n become undistinguishable from $\Delta_0(\omega_m)$ at any $\omega_m > 0$, while the solutions with $n \to \infty$ form a continuous spectrum $\Delta_\xi(\omega_m)$. A continuous ξ is the product of n and $2 - \gamma$, and its value is determined by how the double limit $n \to \infty$ and $\gamma \to 2$ is taken. This is similar to how a continuous phonon spectrum emerges in the thermodynamic limit from a discrete set of energy levels. The condensation energy $E_{c,\xi}$ also becomes a continuous function of ξ. A visual picture is that an infinite set of $E_{c,n}$ approaches $E_{c,0}$ at $\gamma \to 2$ and touches it at $\gamma = 2$–0 [Fig. 1(a) and 1(b)]. This creates a branch of gapless "longitudinal" fluctuations. We argued that these fluctuations destroy phase coherence at any $T > 0$ and give rise to pseudogap behavior at $0 < T < T_p$, where $T_p \sim \bar{g}$ is a would be transition temperature if the solutions with $n > 0$ didn't exist. Away from a QCP, when a pairing boson has a gap ω_D, the superconducting temperature $T_c \propto \omega_D$. This last result applies to electron-phonon pairing at small ω_D.

(6) Extra information about critical behavior emerging at $\gamma \to 2$ comes from the analysis of the gap equation on the real axis. Here, $V(\Omega) \propto e^{i\pi\gamma/2}$ is complex and hence $\Delta_0(\omega)$ is also complex. For $\gamma < 1$, $\mathrm{Re}V(\Omega) \propto \cos\pi\gamma/2$ is positive (attractive), and $\mathrm{Re}\Delta_0(\omega)$ is a regular, sign-preserving function of ω. The corresponding density of states (DOS) vanishes at $\omega < \Delta$ and is nonzero for larger frequencies, as is expected on general grounds for the case when the pairing boson is massless. For $\gamma > 1$, $\mathrm{Re}V(\Omega)$ changes sign. We found that in this situation there appears a finite frequency range where the phase $\eta_0(\omega)$ of $\Delta_0(\omega) = |\Delta_0(\omega)|e^{i\eta_0(\omega)}$ winds up by $2\pi m$, where m is an integer. The value of m increases in increments of one at $\gamma > 1$, and the increase accelerates as γ approaches 2. As the consequence, the DOS develops a set of maxima and minima in the range where the phase winds up. We extended $\Delta_0(z)$ to complex z in the upper half-plane

and traced the phase winding $2\pi m$ to the emergence of m vortices at complex z; each vortex moves from the lower to the upper frequency half-plane as γ increases, leaving a 2π phase winding along the real axis. At $\gamma = 2$, the number of vortices becomes infinite and the frequency range, where $\eta_0(\omega)$ winds up, extends to an infinity, where $\Delta_0(z)$ develops an essential singularity. Its presence is a must as otherwise an extension from an infinite set of vortex points would give $\Delta_0(z) = 0$. In explicit form, the gap function along the real frequency axis at $\gamma = 2$ is $\Delta_0(\omega) \sim \omega/\sin\phi_0(\omega + i\delta)$, where $\phi_0(x)$ is an increasing function of the argument [6–8]. The DOS for such $\Delta_0(\omega)$ consists of a set of δ-functional peaks at frequencies where $\sin\phi_0(\omega) = \pm 1$. This is qualitatively different from a continuum DOS for $\gamma < 2$. This clearly indicates that the $\gamma = 2$ model is critical.

In this paper, we analyze the gap equation on the other side of the critical point, at $\gamma > 2$. We show that at low enough T, the system has long-range superconducting order, the spectrum of the condensation energy is a discrete one, and $E_{c,n}$ with $n > 0$ bounce back, recreating the gap between the largest $E_{c,0}$ and other $E_{c,n}$ [Fig. 1(c)]. This mirrors the case $\gamma < 2$. However, we show that superconducting states at $\gamma < 2$ and $\gamma > 2$ are topologically different as the gap functions in these two cases live on different sheets of the Riemann surface.

The evidence for the topological distinction comes from the analysis of the analytic structure of the gap function $\Delta_0(z)$ in the complex plane of frequency, at $z = \omega' + i\omega''$. Causality requires $\Delta_0(z)$ to be analytic in the upper half-plane. We solve for $\Delta_0(\omega_m)$ on the Matsubara axis and extend the gap function to complex z using Pade approximants (with high enough accuracy to reproduce the known $\Delta_0(\omega)$ along the real axis for $\gamma = 2$). For $\gamma < 2$, the resulting $\Delta_0(z)$ is analytic in the upper half-plane of frequency and has poles in the lower half-plane, i.e. is the correct gap function. For $\gamma > 2$, the gap function obtained this way, which we label as $\tilde{\Delta}_0(z)$, is analytic in the lower half-plane and has poles in the upper half-plane. To obtain the correct $\Delta_0(z)$ one then needs to "invert" the lower and the upper half-planes. In practice this is achieved by taking $\Delta_0(\omega)$ immediately above the real axis to be $\tilde{\Delta}_0^*(\omega)$ immediately below the real axis, that is, by moving the gap function onto a different sheet of the Riemann surface upon crossing from the lower to the upper half-plane. Because $\tilde{\Delta}_0^*(z)$ is analytic in the lower half-plane, Kramers-Kronig relations between $\Delta_0'(\omega)$ and $\Delta_0''(\omega)$ are satisfied. The analytic $\Delta_0(z)$ is then obtained by continuing $\Delta_0(\omega)$ into the upper half-plane using Cauchy relation. In practice, this implies that in the upper half-plane, $\Delta_0(z) = [\tilde{\Delta}(z^*)]^*$. We present complimentary evidence for the transformation of the $n = 0$ gap function onto a different sheet of the Riemann surface from the analytical analysis of $\Delta_0(\omega)$ on the real axis.

We show that only the $n = 0$ gap function moves to a different sheet of the Riemann surface. The functions $\Delta_n(z)$ with $n > 0$ remain on the same sheet of the Riemann surface for $\gamma < 2$ and $\gamma > 2$. This separation between $n = 0$ and $n > 0$ leads to peculiar behavior of the condensation energies $E_{c,n}$ with γ. Namely, for $\gamma < 2$, all $E_{c,n}$ vanish simultaneously once the pairing interaction reduces below a certain threshold; for $\gamma > 2$, $E_{c,n}$ with $n > 0$ vanish at the threshold, but $E_{c,0}$ remains finite, i.e., the $n = 0$ solution survives when all other solutions vanish.

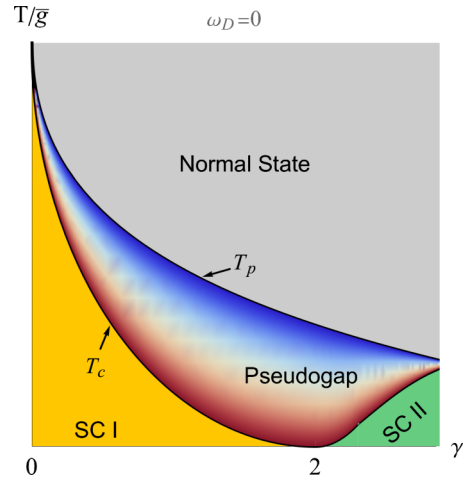

FIG. 2. Phase diagram in variables T and γ for $0 \leqslant \gamma < 3$ and $\omega_D = 0$. There are two topologically distinct superconducting phases SC I and SC II, in which the gap functions live on different sheets of the Riemann surface, and a nonsuperconducting phase with preformed pairs in between.

Our key result is that the topological distinction between $\gamma < 2$ and $\gamma > 2$ gives rise to the measurable effect—the DOS at $\gamma > 2$ develops a nonintegrable singularity (an "infinite" peak) at the lower edge of the continuum. This edge singularity can be interpreted as a bound state between a fermion and a pairing field [6]. For a lattice system with a finite total number of states, the total weight of the edge singularity is finite, but is a fraction the total number of states in the system, i.e., the bound state is macroscopically degenerate.

We extend the analysis of the gap function and the DOS to the case when a boson has a finite mass, which we label as ω_D by analogy with the phonon case. We show that the "infinite" peak survives up to a finite ω_D, i.e., the new structure is stable against small perturbations and occupies a finite region in the phase diagram.

The phase diagrams for the γ model in variables (T, γ) at $\omega_D = 0$ and in (ω_D, γ) at $T = 0$ are shown in Figs. 2 and 3 (see also Fig. 27 below). To obtain these phase diagrams, we combined the results for $\gamma > 2$ with the results for $0 \leqslant \gamma \leqslant 2$ of previous papers from the series, Refs. [1–5]. At $T = 0$, the two superconducting phases SC I and SC II merge at the critical $\gamma = 2$. SC I is a superconducting phase with conventional properties, and SC II is the new SC state with edge singularity in the DOS. At a finite temperature, there is an intermediate regime between the two ordered phases, where long range superconducting order is destroyed by "longitudinal" gap fluctuations, associated with the presence of an infinite set of low-energy local minima in the condensation energy. In this regime, fermions form bound pairs, but the pairs remain incoherent and do not superconduct. The observables in this regime display pseudogap behavior, e.g., fermionic spectral function has a peak at the gap value, but the spectral weight below the gap remains finite.

The structure of the paper is the following. In the next section, we briefly review the γ model and present the gap

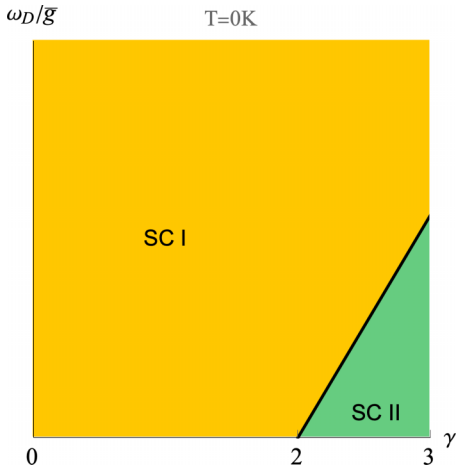

FIG. 3. The phase diagram in variables ω_D and γ at $T = 0K$. There is a single line of a topological transition, which emerges at $\omega_D = 0$ and $\gamma = 2$. The DOS in SC II has a nonintegrable edge singularity.

equation along the Matsubara axis and in real frequencies. In Sec. III, we analyze the gap equation along the Matsubara axis and show that for $\gamma > 2$ it still has an infinite number of topologically distinct solutions, $\Delta_n(\omega_m)$, with $n = 0,\ 1,\ 2\ldots$, like for smaller γ. We present the exact solution of the linearized gap equation, $\Delta_\infty(\omega_m)$, in Sec. III A 2 we discuss the structure of the $n = 0$ solution. In Sec. III A 3 we use the results of Sec. III A 1 to obtain discrete solutions of the nonlinear gap equation, $\Delta_n(\omega_m)$ (Sec. III A 3). In Sec. III B, we extend the model to nonequal interactions in particle-hole and particle-particle channels, taking special care to avoid introducing unphysical divergencies. We show that for $\gamma < 2$, all $\Delta_n(\omega_m)$ disappear once the pairing interaction drops below a certain threshold, while for $\gamma > 2$, the solutions with $n > 0$ disappear at the threshold, but the one with $n = 0$ survives. In Sec. IV, we extend the gap function from the Matsubara axis into the complex plane of frequency and discuss how the $n = 0$ solution moves into a different sheet of the Riemann surface at $\gamma > 2$, while the solutions with $n > 0$ remain on the same Riemann surface as for $\gamma < 2$. Here we also discuss the structure of dynamical vortices and the set of topological transitions, when vortices move one by one into the upper half-plane of frequency as $\gamma \to 2$ from either side. In Sec. V, we analyze the analytic gap function $\Delta_0(\omega)$ for $\gamma > 2$ immediately above the real axis, with particular emphasis to its form near $\omega = \omega_0$, where $\Delta_0(\omega) = \omega$. We first present, in Sec. V A, an approximate treatment, in which we replace the integral gap equation by the differential one and keep only the lowest derivatives of $\Delta(\omega)$. We show that at $\omega \sim \omega_0$, $\Delta_0(\omega)$ is entirely real and $\Delta_0(\omega)/\omega - 1$ scales as $(\omega_0 - \omega - i0)^4$. In Sec. V A 1, we obtain the DOS for this $\Delta_0(\omega)$ and show that it has an infinite peak at ω_0. In Sec. V B, we present more accurate treatment, in which we include higher-order derivatives of $\Delta_0(\omega)$. We show that the form of $\Delta_0(\omega)$ near ω_0 get modified, yet the DOS still has a nonintegrable singularity. In Sec. V C, we show that the singularity in the DOS can be extracted directly from the integral gap equation. In Sec. VI, we extend the analysis to finite mass of a boson and show that the singularity in the DOS survives in a finite range of ω_D. We summarize our results in Sec. VII, combine them with earlier results for smaller γ, and present the phase diagram of the γ model. The phase diagram in (T, γ) plane contains two different superconducting phases and an intermediate regime of preformed pairs with pseudogap behavior of observables.

Some technical details of calculations are moved to the Appendices. Throughout the paper we use ω_m for fermionic frequency along the Matsubara axis (a continuous variable at $T = 0$ and a discrete one at a finite T, $\omega_m = \pi T(2m + 1)$), ω for fermionic frequency along the real axis, and $z = \omega' + i\omega''$, $\omega'' > 0$, for complex frequency in the upper half-plane. We use the notation $\Delta_0(z)$ for the $n = 0$ gap function both for $\gamma < 2$ and $\gamma > 2$ with the understanding that these gap functions live on different sheets of the Riemann surface.

II. MODEL AND ELIASHBERG EQUATIONS

The γ model is an effective model that describes low-energy fermions with dynamical interaction $V(\Omega_m) \propto 1/|\Omega_m|^\gamma$. This model is obtained from an underlying model of itinerant dispersion-full fermions with interaction mediated by a soft boson near a charge or spin QCP, after one integrates over momenta in the expressions for the fermionic self-energy and the pairing vertex. When collective bosons are slow modes compared to fermions (e.g., when they are Landau overdamped by fermions), the momentum integration factorizes between the one transverse to the Fermi surface, which involves only fermionic propagators, and the one along the Fermi surface, which involves the bosonic propagator between points on the Fermi surface and converts it into the local propagator. At a QCP, the local bosonic propagator is massless, and its frequency dependence is singular, $1/|\Omega_m|^\gamma$. The dimensionless interaction, mediated by this boson, is then $V(\Omega_m) = \bar{g}^\gamma/|\Omega_m|^\gamma$, where $\bar{g}$ is the effective fermion-boson coupling constant. The exponent γ is determined by the type of the underlying microscopic model. We refer a reader to paper I for the list of specific examples [1].

The interaction $V(\Omega_m)$ is sign-preserving on the Matsubara axis and singular at $\Omega_m \to 0$. It gives rise to two competing effects: (i) a NFL behavior in the normal state and (ii) an attraction in one or more pairing channels (chosen within the original model with momentum and frequency-dependent interaction). The two trends are described by coupled equations for the fermionic self-energy $\Sigma(\omega_m)$ and the pairing vertex $\Phi(\omega_m)$ (see papers I–IV for the exact forms of these equations). One can replace these two equations by the equation for the pairing gap $\Delta(\omega_m) = \Phi(\omega_m)/(1 + \Sigma(\omega_m)/\omega_m)$ and the inverse quasiparticle residue $Z(\omega_m) = 1 + \Sigma(\omega_m)/\omega_m$. One advantage of using Δ instead of Φ is that the equation for $\Delta(\omega_m)$ can be expressed solely in terms of $\Delta(\omega_{m'})$. In explicit form, the nonlinear gap equation is

$$\Delta(\omega_m) = \bar{g}^\gamma \pi T \sum_{\omega_{m'}} \frac{\Delta(\omega_{m'}) - \Delta(\omega_m)\frac{\omega_{m'}}{\omega_m}}{\sqrt{(\omega_{m'})^2 + \Delta^2(\omega_{m'})}} \frac{1}{|\omega_{m'} - \omega_m|^\gamma}, \quad (1)$$

Another advantage of using Δ instead of Φ is that a potentially singular contribution from $V(\Omega_m \to 0)$, i.e., from $\omega_{m'} \to \omega_m$, is eliminated by vanishing numerator. The cancellation holds both at a finite T and at $T = 0$. At a finite T, the would

be divergent contribution comes from the term with $m' = m$ in the summation over discrete m'. It vanishes, because the numerator vanishes exactly at $m = m'$, and this holds even if we keep a small mass in the bosonic propagator in intermediate calculations. We note in passing that the term with $V(0)$ describes thermal fluctuations, whose role for the pairing parallels that of non-magnetic impurities. The cancellation of the thermal contribution can then be viewed as a realization of the Anderson theorem. At $T = 0$, the integral $\int d\omega'/|\omega - \omega'|^\gamma$ is singular for $\gamma > 1$, but the singular behavior is eliminated as the expansion of the numerator yields compensating $(\omega - \omega')^2$. The frequency integral then remains convergent as long as $\gamma < 3$, which we consider here.

At the onset of the pairing, when $\Delta(\omega_m)$ is infinitesimally small, the gap equation reduces to

$$\Delta(\omega_m) = \bar{g}^\gamma \pi T \sum_{\omega'_m} \left(\frac{\Delta(\omega'_m)}{\omega'_m} - \frac{\Delta(\omega_m)}{\omega_m} \right) \frac{\mathrm{sgn}(\omega_m)}{|\omega'_m - \omega_m|^\gamma}. \quad (2)$$

At zero temperature, one can replace the sum over ω'_m in (1) and (2) by the integral $\pi T \sum_{\omega'_m} \to (1/2) \int d\omega'_m$.

The gap equation on the real axis is obtained by applying spectral representation to Eq. (1) [see Refs. [6,7,9] and papers I, IV, and V for details]. It takes the form

$$\Delta(\omega) B(\omega) = A(\omega) + C(\omega), \quad (3)$$

where the functions $A(\omega)$, $B(\omega)$, and $C(\omega)$ are given by Eqs. (18) and (19) in Sec. V along with Fig. 4.

III. SOLUTION OF THE GAP EQUATION ALONG THE MATSUBARA AXIS

In this section, we present two sets of results. First, we show that at $T = 0$, there exists an infinite number of topologically distinct solutions of the nonlinear gap equation. We label these solutions as $\Delta_n(\omega_m)$, where an integer n indicates how many times $\Delta_n(\omega_m)$ changes sign along the positive Matsubara axis. We recall that we previously found that an infinite discrete set of solutions exists for $0 < \gamma < 2$ (papers I–IV) and becomes continuous at $\gamma = 2$ (paper V). Here we show that the set again becomes a discrete one for $\gamma > 2$. In simple words, condensation energies $E_{c,n}$ with $n > 0$ come closer to $E_{c,0}$ as γ approaches 2, "touch" it at $\gamma = 2$, where the condensation energy becomes a continuous function, and then pull back at larger γ, leaving $E_{c,0}$ the largest and separated by the gap from other $E_{c,n}$. Second, we show that the behavior of $\Delta_0(\omega_m)$ before and after "touching" is qualitatively different. Namely, for $\gamma < 2$, $\Delta_0(\omega)$ disappears simultaneously with other $\Delta_n(\omega_m)$ once the pairing interaction drops below some critical value. For $\gamma > 2$, $\Delta_0(\omega)$ remains nonzero when all other $\Delta_n(\omega_m)$ vanish. To demonstrate this explicitly, we extend the model and introduce a parameter M, which distinguishes between the strength of the interaction in the particle-particle and the particle-hole channel ($M = 1$ in the original model). For $\gamma < 2$, $\Delta_n(\omega_m)$ with all n, including $n = 0$, vanish for $M < M_{\mathrm{cr}}(\gamma)$ [see Eq. (12)]. For $\gamma > 2$, $\Delta_n(\omega_m)$ with $n > 0$ still vanish for $M < M_{\mathrm{cr}}(\gamma)$, but $\Delta_0(\omega_m)$ remains finite down to $M = 0$ and vanishes there in a highly nontrivial manner. Later, in Sec. V, we analyze the gap function on the real axis and show that the $n = 0$ solution does change qualitatively compared to that for $\gamma < 2$ and yields qualitatively different structure of the density of states.

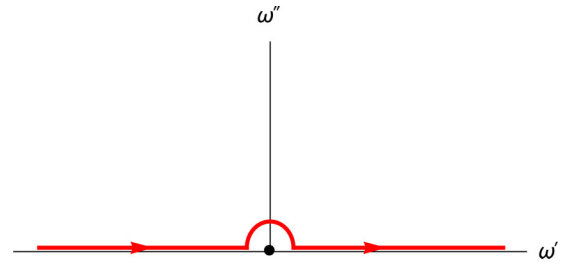

FIG. 4. The integration contour for $C(\omega)$ in Eq. (19) for $\gamma > 2$. The contour bypasses the point $\Omega_m = 0$, where the interaction $V(\omega)$ is singular and $\int d\Omega \Omega \mathrm{Im} V(\omega)$ diverges.

A. Discrete set of $\Delta_n(\omega_m)$ for $\gamma > 2$

1. Solution of the linearized gap equation

We begin by showing that the solution of the linearized gap equation at $T = 0$ still exists for $\gamma > 2$, like for smaller γ. We label this solution $\Delta_\infty(\omega_m)$ as the corresponding gap function changes sign an infinite number of times as a function of ω_m.

At $T = 0$, the linearized gap equation (2) reads

$$\Delta_\infty(\omega_m) = \frac{\bar{g}^\gamma}{2} \int_{-\infty}^{\infty} d\omega_{m'} \left(\frac{\Delta_\infty(\omega_{m'})}{\omega_{m'}} - \frac{\Delta_\infty(\omega_m)}{\omega_m} \right) \times \frac{\mathrm{sgn}(\omega_{m'})}{|\omega_{m'} - \omega_m|^\gamma}. \quad (4)$$

Candidate solutions of this equation can be identified analytically at frequencies much larger and much smaller than $\bar{g}$. At large $\omega_m \gg \bar{g}$, one can pull out $1/|\omega_m|^\gamma$ from the integral and obtain $\Delta_\infty(\omega_m) \propto 1/|\omega_m|^\gamma$. At small $\omega_m \ll \bar{g}$, the solution is a combination of two power-laws $\Delta(\omega_m) \propto |\omega_m|^{a_{1,2}}$. Substituting this form into (4) we find the condition on a:

$$\int_{-\infty}^{\infty} dx \frac{|x|^a - \mathrm{sgn}(x)}{|x - 1|^\gamma} = 0. \quad (5)$$

For $\gamma \leqslant \gamma_{\mathrm{cr}} \simeq 2.81$, $a_{1,2}$ are complex-conjugated numbers, $\gamma/2 \pm i\gamma\beta$, where β is determined from

$$\frac{1 - \gamma}{2} \frac{\Gamma\left(\frac{\gamma}{2} + i\beta\gamma\right)\Gamma\left(\frac{\gamma}{2} - i\beta\gamma\right)}{\Gamma(\gamma)} \left(1 + \frac{\cosh(\pi\gamma\beta)}{\cos(\pi\gamma/2)} \right) = 1. \quad (6)$$

(γ_{cr} is the solution of this equation for $\beta = 0$). We plot $\beta = \beta(\gamma)$ in Fig. 5. The gap function $\Delta_\infty(\omega_m) = |\omega_m|^{\gamma/2}(C|\omega|^{i\gamma\beta} + C^*|\omega|^{-i\gamma\beta})$ oscillates as a function of $\ln|\omega_m|$ as ($C = |C|e^{i\phi}$)

$$\Delta_\infty(\omega_m \ll \bar{g}) = |C||\omega_m|^{\gamma/2} \cos(\beta \ln|\omega_m| + \phi), \quad (7)$$

where ϕ is a free phase factor in this approximation. The infrared behavior is the same as we previously found for smaller γ. It is tempting to use ϕ as a tool that allows one to smoothly connect the limits of large and small ω_m. There is no guarantee that this is possible as the gap equation is integral rather than differential. In papers I–V, we went a step further and obtained the exact solution of the linearized gap equation at $T = 0$. It reproduces $1/|\omega_m|^\gamma$ behavior at

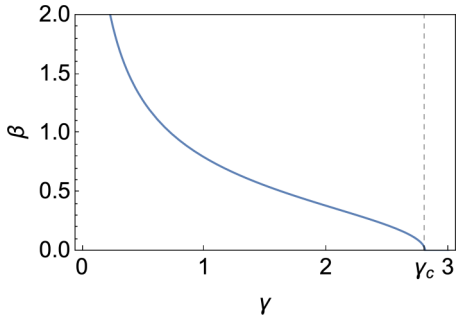

FIG. 5. The parameter β, which sets the periodicity of logarithmic oscillation of $\Delta_\infty(\omega_m)$ at the smallest ω_m, as a function of γ. It remains nonzero up to critical $\gamma_{cr} \simeq 2.81$.

large ω_m and log-oscillations at small ω_m with some particular ϕ. This eventually allows us to obtain a discrete set of solutions of the nonlinear gap equation, $\Delta_n(\omega_m)$, in which $\Delta_\infty(\omega_m)$ is the smallest member. Here, we borrowed computational technique from papers I-V and obtained the exact solution $\Delta_\infty(\omega_m)$ for $\gamma > 2$ (up to $\gamma_{cr} = 2.81$). The exact solution again matches with analytical high-frequency and small-frequency forms, with some γ-dependent parameter ϕ. We show $\Delta_\infty(\omega_m)$ for representative $\gamma = 2.5$ in Fig. 6. Note that because logarithmic oscillations extend down to $\omega_m = 0$, $\Delta_\infty(\omega_m)$ changes sign an infinite number of times, what justifies labeling it as $n = \infty$ solution.

2. Sign-preserving solution

We now consider the opposite limit–the sign-preserving, $n = 0$ solution of the nonlinear gap equation. We obtained this solution numerically and show the results in Fig. 7. In Fig. 7(a), we show $\Delta_0(\omega_m)$ for several representative $2 < \gamma < 3$. We see that the $\Delta_0(\omega_m)$ has a finite value at $\omega_m = 0$ and monotonically decreases with increasing ω_m. This is similar to the behavior of $\Delta_0(\omega_m)$ at smaller γ. In Fig. 7(b), we show $\Delta_0(0)$ versus γ. For a generic γ between 2 and 3, $\Delta_0(0) \sim \bar{g}$. At $\gamma \to 3$, $\Delta_0(0)$ diverges logarithmically (Ref. [10]). For completeness, in Figs. 7(c) and 7(d) we show the corresponding onset temperature for the pairing $T_{p,0}$ and the ratio

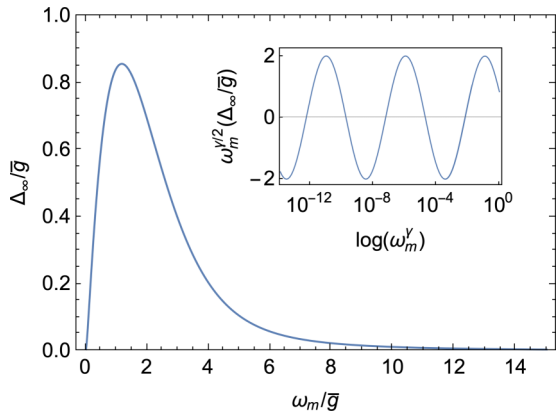

FIG. 6. The gap function $\Delta_\infty(\omega_m)$ along the Matsubara axis, for $\gamma = 2.5$. The inset shows logarithmic oscillations in the infrared limit.

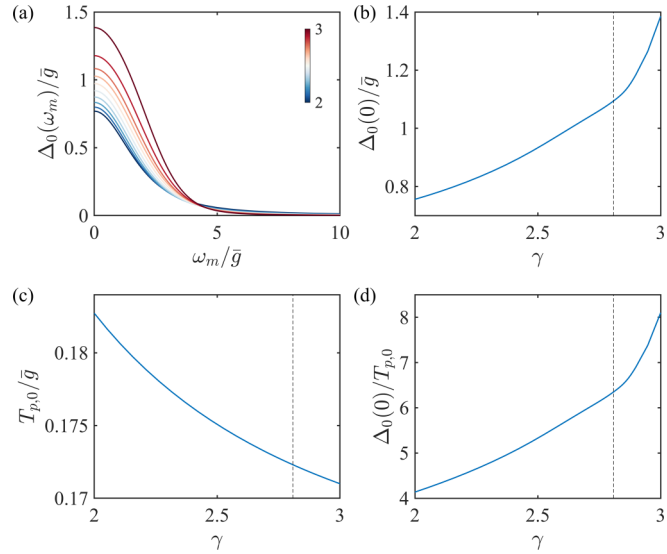

FIG. 7. (a) The numerical solution for the gap function $\Delta_0(\omega_m)$ for $2 < \gamma < 3$ at temperature $T = 10^{-3}\bar{g}$. [(b)–(d)] The amplitude of $\Delta_0(0)$, the onset temperature $T_{p,0}$, and the ratio $\Delta_0(0)/T_{p,0}$ as functions of γ. The dashed vertical line marks the critical γ_{cr}, above which the solutions with $n > 0$ do not exist.

$\Delta_0(0)/T_{p,0}$. The results are consistent with what has been reported earlier [10,11]. At large frequencies, $\Delta_0(\omega_m)$ scales as $1/|\omega_m|^\gamma$. This form can be straightforwardly extracted from the gap equation in the same way as for the $n = \infty$ solution, by pulling out $1/|\omega_m|^\gamma$ from the integrand. For the $n = 0$ solution, this gives

$$\Delta_0(\omega_m) = Q_{\gamma,0}\left(\frac{\bar{g}}{|\omega_m|}\right)^\gamma, \tag{8}$$

where

$$Q_{\gamma,0} = \int_0^\infty \frac{d\omega_m' \Delta_0(\omega_m')}{\sqrt{\Delta_0^2(\omega_m') + (\omega_m')^2}}. \tag{9}$$

Substituting $\Delta_0(\omega_m) \propto 1/|\omega_m|^\gamma$, we find that the integral is ultra-violet convergent, what justifies pulling out $1/|\omega_m|^\gamma$. For a generic γ between 2 and 3, the frequency integral in (9) converges at $\omega_m' \sim \Delta_0(0) \sim \bar{g}$, hence $Q_{\gamma,0}$ is of order $\bar{g}$. We show $Q_{\gamma,0}$ in Fig. 8. We see that it is indeed of order $\bar{g}$.

3. Discrete set of solutions

For $\gamma < 2$, we showed in papers I–IV that $\Delta_\infty(\omega_m)$ and $\Delta_0(\omega_m)$ are the two end points of an infinite discrete set of solutions $\Delta_n(\omega_m)$. A gap function labeled by n changes sign n times along the positive Matsubara axis. The set becomes continuous at $\gamma = 2$ (paper V). Here we show that an infinite set of $\Delta_n(\omega_m)$ exists also for $\gamma > 2$, but again becomes discrete.

To demonstrate this, we search for the solution of the nonlinear gap equation by expanding to infinite order in $\Delta(\omega_{m'})$ in Eq. (1). This yields

$$\Delta(\omega_m) = \sum_{j=0}^{\infty} \epsilon^{2j+1} \Delta^{(2j+1)}(\omega_m), \tag{10}$$

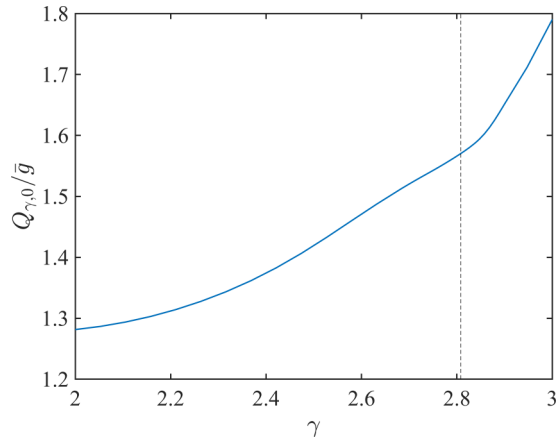

FIG. 8. $Q_{\gamma,0}$, defined in Eq. (9), as a function of $\gamma \in (2, 3)$. We used $\Delta_0(\omega_m)$ from Fig. 7 as an input or the calculation of $Q_{\gamma,0}$. The dashed vertical line marks $\gamma_c = 2.81$.

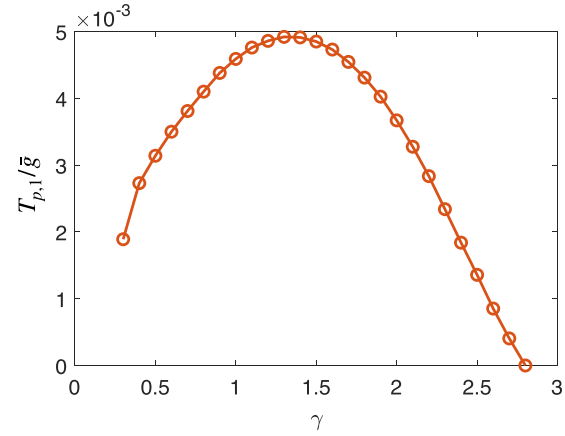

FIG. 9. The temperature $T_{p,1}$, below which the $n = 1$ solution appears, as a function of γ. Observe that $T_{p,1}$ is a nonmonotonic function of γ. It initially increases with γ, reaches a maximum at $\gamma \geqslant 1$, and then decreases and vanishes at $\gamma = \gamma_{\rm cr} = 2.81$. The onset temperatures $T_{p,n}$ with $n > 1$ show similar behavior.

where $\Delta^{(1)}(\omega_m) = \Delta_\infty(\omega_m)$ from Eq. (7), ϵ is a parameter, which we adjust to get a solution. The two limits we considered earlier correspond to an infinitesimally small ϵ, when $\Delta(\omega_m) = \epsilon\Delta_\infty(\omega_m)$, and to some finite $\epsilon = \epsilon_0$ for the $n = 0$ solution.

In general, the conditions on ϵ are obtained by substituting $\Delta(\omega_m)$ from Eq. (10) into Eq. (1), solving iteratively for $\Delta^{(2j+1)}$ in terms of $\Delta^{(2j'+1)}$ and $j' < j$, and requiring that the series converge. For a BCS superconductor, the solution exists only for a single value of ϵ. For the γ model with $\gamma \leqslant 2$, the solutions exist for a discrete set of ϵ_n for $\gamma < 2$ and for arbitrary $0 < \epsilon < \epsilon_{max}$ for $\gamma = 2$.

For $\gamma > 2$, we find that the solutions exist for a discrete set of ϵ_n, of which ϵ_0 is the largest. This is very similar to the case $\gamma < 2$. The details of the calculations are rather involved and we moved them to Appendix E.

We also compute the condensation energy for different solutions using the expression for the free energy in the γ model in paper I. The set of condensation energies $E_{c,n}$ is discrete, and, as one could expect, the largest condensation energy is for the $n = 0$ solution. This again is very similar to what we previously found for $\gamma < 2$. We illustrate this in Fig. 1(c).

B. Decoupling of the $n = 0$ solution from the set

So far, our results for $\gamma > 2$ parallel those for $\gamma < 2$. In both cases, there exists a discrete set of $\Delta_n(\omega_m)$ with integer n, ranging from 0 to ∞. Each solution corresponds to a local minimum in the condensation energy, and $E_{c,0}$ is the largest.

We now show that the analogy is only partially correct, and there is one crucial feature on which the two cases differ qualitatively. Namely, we argue that for $\gamma < 2$, the solutions with all n behave as one set, while for $\gamma > 2$, the $n = 0$ solution decouples from the set and behaves differently from the solutions with $n > 0$. What we mean here is that for smaller γ, all $\Delta_n(0)$ disappear simultaneously once we extend the model and reduce the strength of the pairing interaction below a certain value (more on this below). For $\gamma > 2$, the solutions with $n > 0$ disappear under the same conditions, but the one with $n = 0$ survives. This distinction can be seen already in the original γ model. As we said before, the solution with $n = \infty$ exists only up to $\gamma_{\rm cr} = 2.81$ [12]. We argue that all solutions with noninfinite $n > 0$ also disappear at this γ. To prove this, we compute the corresponding onset pairing temperatures $T_{p,n}$. In Fig. 9, we plot $T_{p,1}$ as a function of γ. We see that it vanishes at $\gamma = \gamma_{\rm cr}$. We verified that $T_{p,2}$ vanishes as well. This leaves little doubt that all $T_{p,n}$ with $n > 0$ vanish at $\gamma_{\rm cr}$. The vanishing of $T_{p,n>0}$ in turn implies that at $T = 0$ all $\Delta_{n>0}(\omega_m)$ also vanish simultaneously at $\gamma_{\rm cr}$. However, we see from Figs. 7(b) and 7(c) that $T_{p,0}$ and the gap function $\Delta_0(\omega_m)$ at $T = 0$ remain finite at this γ, the only signature of $\gamma_{\rm cr}$ in these figures is a kink in the γ dependence of $T_{p,0}$ and of $\Delta_0(0)$. Clearly then, the $n = 0$ solution decouples from the set of $\Delta_n(\omega_m)$ with $n > 0$.

1. *Extended γ model*

To see this more clearly and also to understand the difference between $\gamma < 2$ and $\gamma > 2$, we extend the γ model in the same way as in papers IV and V, by introducing a parameter $M \neq 1$, which separates the pairing interaction and the one in the particle-hole channel. The original γ model, in which both interactions are $V(\Omega_m)$, corresponds to $M = 1$. We introduce $M \neq 1$ in such a way that the pairing interaction gets weaker at $M < 1$. The extension has to be done carefully to avoid emerging singularities from $\int d\omega_{m'}/|\omega_m - \omega_{m'}|^\gamma$, which cancel out in the gap equation at $M = 1$ [see Eq. (1)].

We already used this extension for different purposes in papers IV and V. There, we derived the modified gap equation:

$$D(\bar{\omega}_m)\left(\bar{\omega}_m + \frac{1-M}{2}\int \frac{d\bar{\omega}'_m}{|\bar{\omega}_m - \bar{\omega}'_m|^\gamma}\left(\frac{\mathrm{sign}\bar{\omega}_m}{\sqrt{1+D^2(\bar{\omega}_m)}} - \frac{\mathrm{sign}\bar{\omega}'_m}{\sqrt{1+D^2(\bar{\omega}'_m)}}\right)\right) = \frac{1}{2}\int \frac{d\bar{\omega}'_m}{|\bar{\omega}_m - \bar{\omega}'_m|^\gamma}\frac{D(\bar{\omega}'_m) - D(\bar{\omega}_m)}{\sqrt{1+D^2(\bar{\omega}'_m)}}\mathrm{sign}\bar{\omega}'_m \tag{11}$$

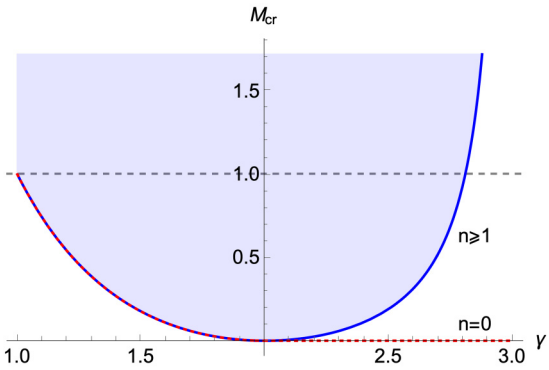

FIG. 10. The critical value of the parameter M in Eq. (11) as a function of γ The gap functions $\Delta_n(\omega_m)$ are nonzero for $M > M_{\rm cr}$. At $\gamma \leqslant 2$, $M_{\rm cr}$ is the same for all $n \geqslant 0$. At $\gamma > 2$, critical M is zero for the $n = 0$ solution (red dots) and is finite for solutions with $n \geqslant 1$ (blue line).

where $D(\bar{\omega}_m) = \Delta(\omega_m)/\omega_m$, $\bar{\omega}_m = \omega_m/\bar{g}_M$ and $\bar{g}_M = \bar{g}/M^{1/\gamma}$. At $M = 1$, Eq. (11) reduces to Eq. (1)

The extended model has the same structure of solutions as the original one: there is a discrete set of solutions $\Delta_n(\omega_m)$ for $\gamma < 2$ and $\gamma > 2$ and a continuous set for $\gamma = 2$. The end point, $\Delta_\infty(\omega_m)$ is the solution of the linearized gap equation. Like for the original model, at small ω_m, $\Delta_\infty(\omega_m) \propto |\omega_m|^{\gamma/2} \cos(\beta \ln|\bar{\omega}_m|^\gamma + \phi)$. The parameter β must be real, which restricts M to $M \geqslant M_{\rm cr}(\gamma)$. The critical value is

$$M_{\rm cr}(\gamma) = \frac{1-\gamma}{2}\frac{\Gamma^2\left(\frac{\gamma}{2}\right)}{\Gamma(\gamma)}\left(1 + \frac{1}{\cos(\pi\gamma/2)}\right). \qquad (12)$$

We plot $M_{\rm cr}$ versus γ in Fig. 10. The solution with $n = \infty$ exists in the blue area in this figure. The boundary crosses $M = 1$ at $\gamma_{\rm cr} = 2.81$, as we found earlier.

We obtained numerically the onset temperatures for the pairing $T_{p,n}(M)$. For $\gamma \leqslant 2$, we found that all $T_{p,n}$ vanish at the same $M = M_{\rm cr}$. This implies at $T = 0$, $\Delta_n(\omega_m)$ with all n, including $n = 0$, vanish upon approaching the critical line $M_{\rm cr}(\gamma)$ from above. We show the behavior of $\Delta_0(\omega_m)$ in Fig. 12(a) and illustrate this result in Fig. 11(a). For $\gamma = 2$, $M_{\rm cr} = 0$. The set is continuous, and all gap functions from the set vanish upon approaching $M_{\rm cr} = 0$ from above [see Fig. 11(b)].

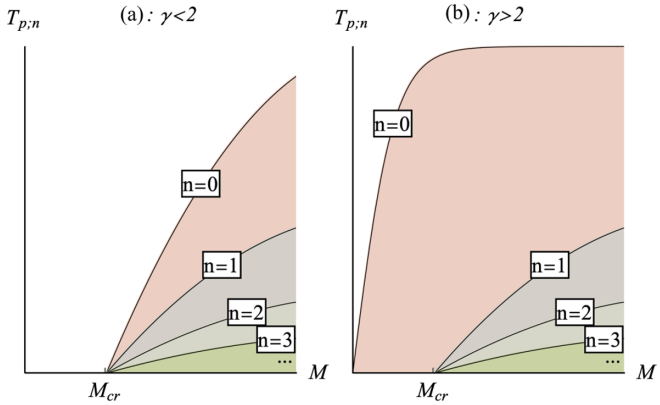

FIG. 11. The onset temperatures $T_{p,n}$ for the gap functions $\Delta_n(\omega_m)$ for (a) $\gamma < 2$ and (b) $\gamma > 2$.

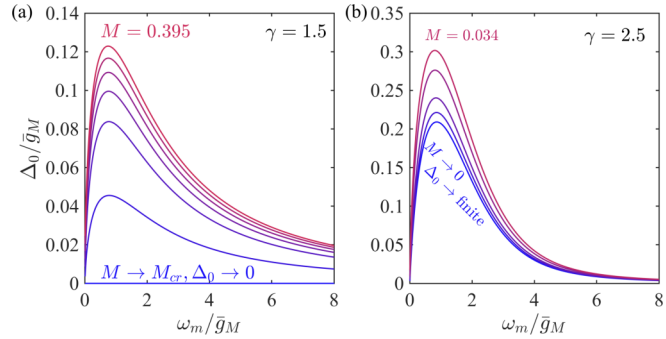

FIG. 12. The gap function $\Delta_0(\omega_m)$, obtained by the numerical solution of Eq. (11), for various values of M and $\gamma = 1.5$ and 2.5, representative of $\gamma < 2$ and $\gamma > 2$, respectively. For $\gamma = 1.5$, $\Delta_0(\omega_m)$ vanishes continuously at $M = M_{\rm cr} > 0$. For $\gamma = 2.5$, it remains finite for all $M > 0$ and vanishes discontinuously at $M = 0$.

For $\gamma > 2$, the result is different. The onset temperatures $T_{p,n}$ with $n > 0$ still vanish at $M_{\rm cr} > 0$, along with the corresponding $\Delta_n(\omega_m)$ at $T = 0$. However, $T_{p,0}$ and $\Delta_0(\omega_m)$ remain finite at $M_{\rm cr}$ [see Fig. 11(b) for illustration]. We show the numerical results for $\Delta_0(\omega_m)$ at different M in Fig. 12(b) for representative $\gamma = 2.5$ ($M_{\rm cr} = 0.192$). This clearly shows that for $\gamma > 2$ the solution with $n = 0$ decouples from the set of solutions with $n \geqslant 1$. A nonzero $\Delta_0(\omega_m)$ exists down to $M = 0$ (see Fig. 10), where it displays rather peculiar critical behavior: $\Delta_0(0)$ gradually tends to zero at $M \to 0$, while the full function $\Delta_0(\omega_m)$ remains finite [see Fig. 12(b)] and at $M = 0+$ becomes the end point of a continuum of solutions (see Appendix F for details).

IV. THE GAP FUNCTIONS $\Delta_n(z)$ AT COMPLEX FREQUENCY

In this section, we argue that the ground states at $\gamma < 2$ and $\gamma > 2$ are topologically different, i.e., $\gamma = 2$ is a quantum-critical point of a topological transition. For this, we extend the functions $\Delta_n(\omega_m)$ from the Matsubara axis into the complex plane of frequency. We first consider the $n = 0$ solution and then other solutions with $n > 0$.

A. The $n = 0$ solution

To begin with, we borrow the results of earlier works [6–9] and our previous analysis for $\gamma \leqslant 2$ in papers IV and V on the evolution of $\Delta_0(\omega) = \Delta_0'(\omega) + i\Delta_0''(\omega)$ at $T = 0$ along the real axis (more accurately, infinitesimally above the real axis). This analysis have shown that as γ approaches 2, $\Delta_0'(\omega)$ undergoes sharp changes near particular ω_k, $k = 1, 2, \ldots$ from large positive to large negative values, while $\Delta''(\omega) \propto (-1)^{k+1}$ sharply increases near these points and gets strongly reduced in between ω_k (see the plots of $\Delta_0(\omega)$ in Fig. 13). A simple experimentation shows that this behavior is reproduced if we set

$$\Delta_0(\omega) \approx A_k \frac{(-1)^k}{\omega - \omega_k + i\gamma_k} \qquad (13)$$

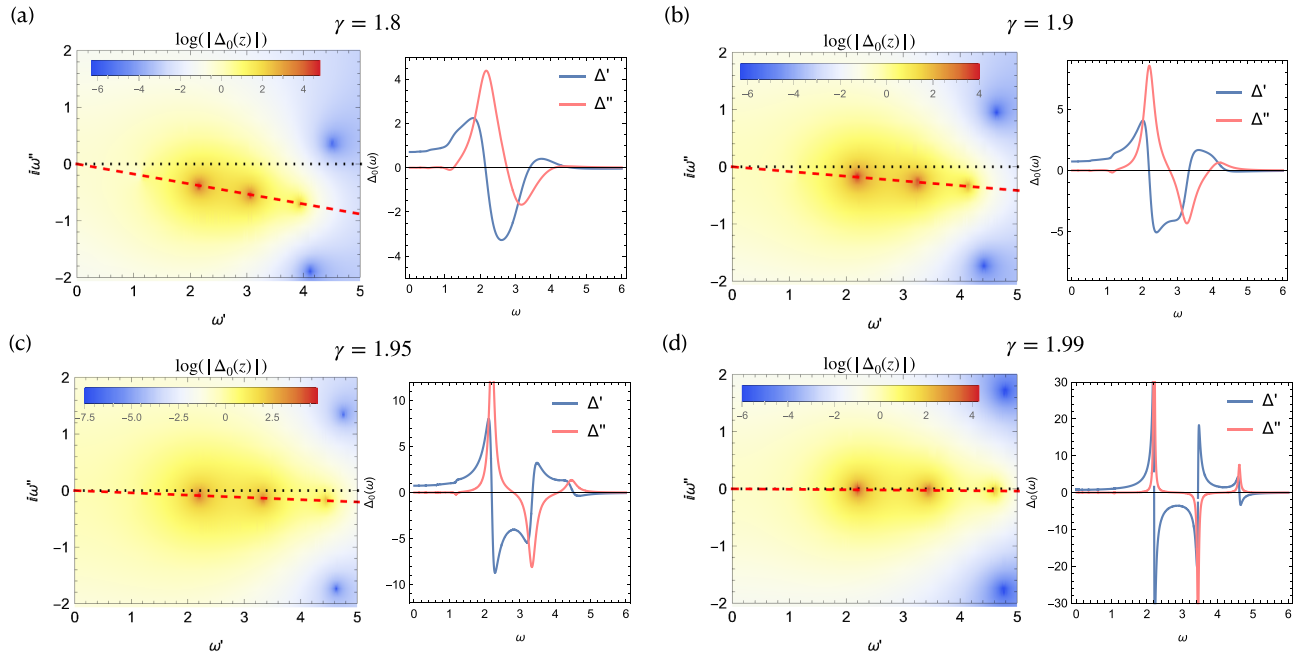

FIG. 13. $\ln(|\Delta_0(z)|)$ in the complex plane of frequency and $\Delta_0'(\omega)$ and $\Delta_0''(\omega)$ along the real axis for several $\gamma \leqslant 2$. The gap function $\Delta_0(z)$ has been obtained by first solving the gap nonlinear gap equation on the Matsubara axis and then extending to complex z using Pade approximants. In the plots of $\ln(|\Delta_0(z)|)$, the red dashed line is along $z = r\exp(i\theta_\gamma)$ with $\theta_\gamma = \pi/2 - \pi/\gamma$. To our numerical accuracy, all poles are on this line. The line of poles rotates towards the real axis as γ approaches 2. Bright blue spots are the positions of zero of $\Delta_0(z)$. The total number of poles and the number of zeros in the first and the fourth quadrants of z must be the same. Along the real axis, both $\Delta_0'(\omega)$ and $\Delta_0''(\omega)$ oscillate with frequency. At $\gamma = 1.99$, the complex function $\Delta_0(\omega)$ is well described by (13).

where $\gamma_k > 0$. Extending this form to the complex plane, we immediately find that $\Delta_0(z)$ has a set of poles in the lower half-plane, at $z = \omega_k - i\gamma_k$. In the left panels in Fig. 13, we show $\ln(|\Delta_0(z)|)$ in the first and fourth quadrants, obtained by high-accuracy Pade approximants [13]. We clearly see that there is a set of poles in the lower half plane. To numerical accuracy, the set is along the line $z'/z'' = \tan\pi/\gamma < 0$. The same plots also show that $\Delta_0(z)$ displays two sets of zeros, surrounding each line of poles. This is consistent with our earlier analysis in paper IV, where we obtained the zeros of $\Delta_0(z)$ in the upper half-plane by analytical continuation from the real axis. The total number of zeros and the poles is the same as one can verify by using the identity $\int d\omega_m[d\ln\Delta_0(\omega_m)/d\omega_m] = 0$ and computing the integral by closing the integration contour over a semicircle in the complex plane in the first and the fourth quadrants [14] We note in passing that as long as $\gamma < 2$, the number of zeros in the upper half-plane is finite. Because each zero gives rise to 2π phase variation on the real axis (see paper IV), the phase winding of $\Delta_0(\omega)$ saturates at large ω, where both $\Delta_0'(\omega)$ and $\Delta_0''(\omega)$ become sign-preserving and scale as $1/\omega^\gamma$.

As γ moves closer to 2, the direction of the line of poles in the lower half-plane moves towards the real axis and γ_k in Eq. (13) get smaller. At $\gamma = 2 - 0$, we have on the real axis $\Delta_0(\omega) = \omega/\sin\phi_0(\omega + i0)$, where $\phi_0(\omega + i0)$ is well approximated by $\phi_0(\omega + i0) = (\omega + i0)^2/(\pi\bar{g}^2)$ at $\omega \geqslant \bar{g}$ (Refs. [5–7]). Expanding near $\omega_k = \pi\bar{g}\sqrt{k}$, we obtain

$$\Delta_0(\omega) \approx \frac{\pi}{2}\frac{(-1)^k}{\omega - \omega_k + i0}. \tag{14}$$

We see that at $\gamma = 2 - 0$, the poles approach the real axis.

We now move to $\gamma > 2$. Let's label the gap function, which gradually evolves from $\gamma < 2$, as $\tilde{\Delta}_0(z)$. By continuity, we expect $\tilde{\Delta}_0(z)$ to possess poles in the upper half-plane. Using Pade approximants we find exactly this behavior: the line of poles is now located in the upper half-plane along the direction $|z'|/z'' = \tan\pi/\gamma > 0$. We show this in Fig. 14. Obviously, this $\tilde{\Delta}_0(z)$ does not satisfy causality. In Fig. 15 we show that the phase of $\tilde{\Delta}_0(\omega)$ winds up along the real axis by multiples of $\%-2\pi$ instead of $+2\pi$.

To obtain the correct gap function $\Delta_0(z)$, analytic in the upper half-plane, we use the fact that while $\tilde{\Delta}_0(z)$ has poles in the upper half-plane, it is analytic in the lower half-plane. For such function, the modified Kramers-Kronig relations and the Cauchy relation between $\Delta_0(\omega_m)$ with $\omega_m < 0$ and $\tilde{\Delta}_0''(\omega)$ immediately below the real axis are

$$\tilde{\Delta}_0'(\omega) = -\frac{1}{\pi}\mathcal{P}\int dx\frac{\tilde{\Delta}_0''(x)}{x-\omega},$$
$$\Delta_0(\omega_m) = -\frac{1}{\pi}\int dx\frac{\tilde{\Delta}_0''(x)}{x - i\omega_m}. \tag{15}$$

Because the gap function on the Matsubara axis is symmetric with respect to $\omega_m \to -\omega_m$, the last relation can be extended to positive ω_m and compared with the original $\tilde{\Delta}_0(\omega_m)$, which we extended to complex plane using Pade approximants. We show in Fig. 16 that the two functions coincide with high accuracy. The near-perfect agreement is a strong indication that there are no additional poles in the lower half-plane.

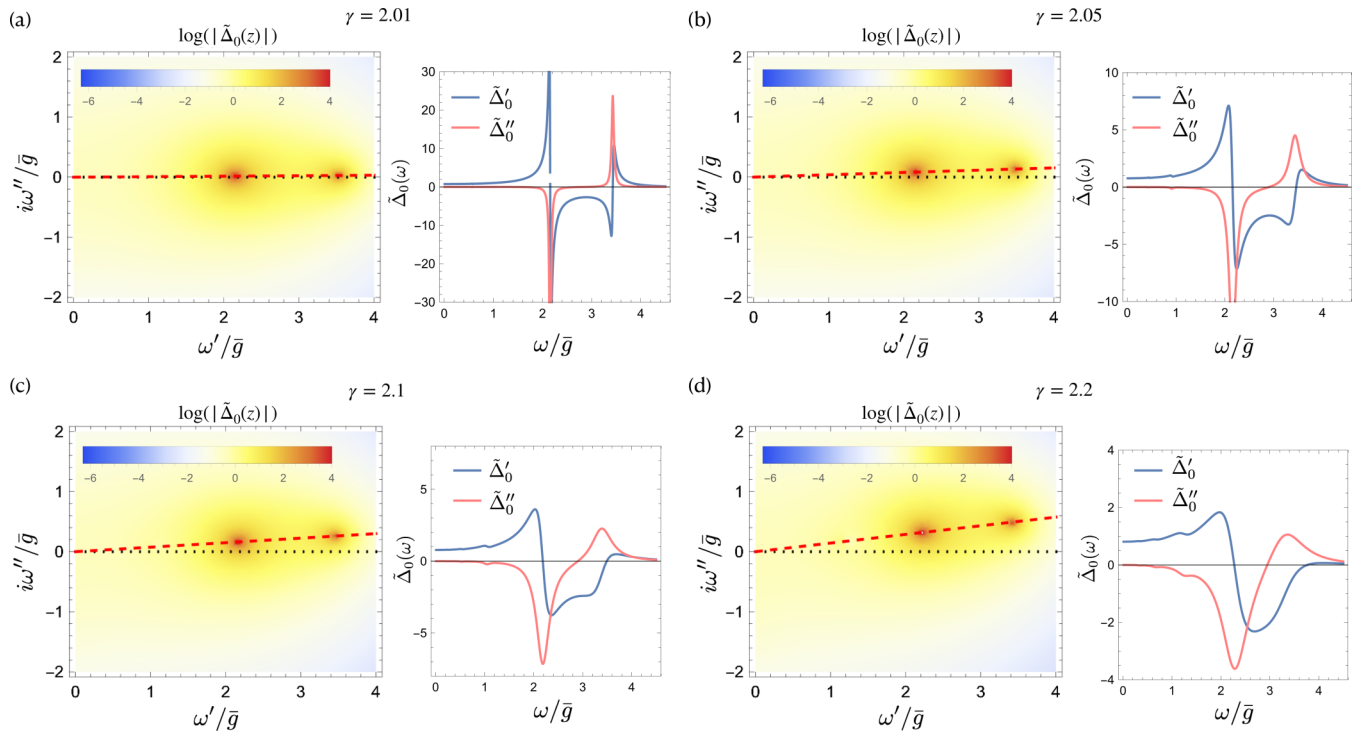

FIG. 14. Same as in Fig. 13, but for $\gamma \geqslant 2$. The function $\tilde{\Delta}_0(z)$ has been obtained from $\Delta_0(\omega_m)$ using Pade approximants. The poles of $\tilde{\Delta}_0(z)$ are along the red dashed line, directed along $|\omega'|/\omega'' = \tan\pi/\gamma > 0$. For $\gamma > 2$, this line is in the upper half-plane. The zeros of $\tilde{\Delta}_0(z)$ below and above the pole line do exist, but are outside the plot range. We argue in the text that the physical gap function $\Delta_0(z) = [\tilde{\Delta}(z^*)]^*$.

Equation (15) suggests a simple way to find the actual $\Delta_0(z)$, analytic in the upper half-plane. For this one has to move to a different sheet of the Riemann surface by choosing $\Delta_0(\omega)$ immediately above the real axis to be equal to $\tilde{\Delta}_0^*(\omega - i0)$, taken immediately below the real axis, and then analytically continue $\Delta_0(\omega)$ into the upper half-plane using the Cauchy relation $\Delta_0(z) = (1/\pi)\int dx \Delta_0''(x)/(x - z)$. Equation (15) ensures that $\Delta_0(z)$ is analytic for $z'' > 0$. One can easily verify that $\Delta_0(z) = [\tilde{\Delta}(z^*)]^*$. In the full complex plane $\Delta_0(z)$ has poles in the lower half-plane along the direction $|z'|/z'' = -\tan\pi/\gamma < 0$ and zeros in both half-planes. As γ increases further, the line of poles of $\Delta_0(z)$ moves deeper into the lower half-plane and the number of zeros in the upper half-plane decreases and vanishes above a certain $\gamma > 2$. In this respect, the behavior of the analytic gap function for $\gamma > 2$ mimics that for $\gamma < 2$. However, the functions $\Delta_0(z)$ at $\gamma < 2$ and $\gamma > 2$ live on different sheets of the Riemann surface and are therefore topologically different, separated by a topological quantum-critical point at $\gamma = 2$. We illustrate this in Fig. 17.

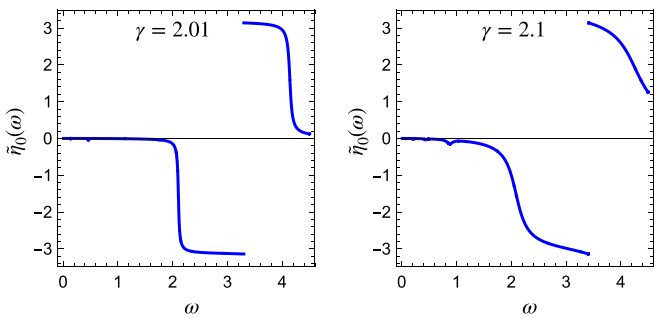

FIG. 15. The variation of the phase of $\tilde{\Delta}_0(\omega) = |\tilde{\Delta}_0(\omega)|e^{i\tilde{\eta}_0(\omega)}$. As the poles of $\tilde{\Delta}_0(z)$ are in the upper half-plane (see Fig. 14), its phase along real axis winds up by multiples of -2π instead of $+2\pi$.

B. The solutions with $n > 0$

We now argue that other $\Delta_n(z)$ with $n > 0$ remain on the same sheet of the Riemann surface through $\gamma = 2$ and therefore for $\gamma > 2$ are located on the different sheet than the $n = 0$ solution. This naturally explains why the $n = 0$ solution survives at above critical $\gamma = 2.81$, when all solutions with $n > 0$ vanish.

To demonstrate this, we consider $\gamma = 2$ and borrow the results of paper V on the structure of the gap functions from the continuum spectrum away from the minimum of the condensation energy. At $\gamma > 2$, these gap functions become the gap functions of discrete states with some $n > 0$.

The states of the continuous spectrum are characterized by a continuous variable ξ. In paper V, we analyzed the form of $\Delta_\xi(\omega)$ along the real axis. At ω larger than $\bar{g}$, we obtained

$$\Delta_\xi(\omega) \approx \frac{\omega}{\sin[\phi(\omega) + i\ln(1+\xi)]}, \tag{16}$$

where $\phi(\omega) \approx \omega^2/(\pi\bar{g}^2)$. At $\xi = 0$, Eq. (16) reduces to $\Delta_0(\omega) = \omega/\sin(\omega^2/(\pi\bar{g}^2))$, which we used in the previous section. At large ξ, $\Delta_\xi(\omega) \propto \omega e^{i\omega^2/(\pi\bar{g}^2)}$ is the solution of the linearized gap equation.

Equation (16) can be straightforwardly extended to the complex plane by just replacing ω by $z = \omega' + i\omega''$. Analyz-

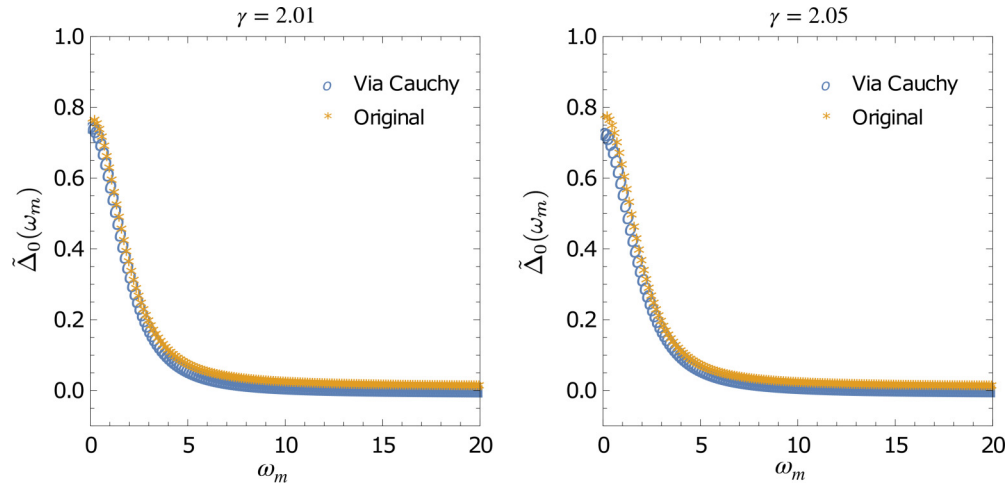

FIG. 16. Comparison between the original $\Delta_0(\omega_m)$ and the one obtained using (15).

ing $\Delta_\xi(z)$, we obtain that it has poles in the lower half-plane, at $z = z_m = a_m + ib_m$, where

$$b_m = -\pi\bar{g}\sqrt{\frac{m}{2}}\left[\left(1+\frac{\ln^2(1+\xi)}{\pi^2 m^2}\right)^{1/2}-1\right]^{1/2},$$
$$a_m = \pm\bar{g}^2\frac{\pi}{2}\frac{\ln(1+\xi)}{b_m}. \tag{17}$$

At small ξ, $b_m \approx -\xi\bar{g}/(2\sqrt{m})$ and $a_m \approx \pm\pi\bar{g}\sqrt{m}$. At large ξ, $b_m \approx -\bar{g}\sqrt{\pi\ln\xi/2}$ and $a_m \approx \pm b_m$ for $m < \ln\xi/\pi$ and $b_m \approx -\bar{g}(\ln\xi)/(2\sqrt{m})$ and $a_m \approx \pm\pi\bar{g}\sqrt{m}$ for $m > (\ln\xi)/\pi$. We show the location of the poles at different ξ in Fig. 18. We see that they are indeed in the lower half-plane, at a finite distance from the real axis.

At smaller $\omega < \bar{g}$, $\Delta_\xi(\omega)$ is given by the series of complex oscillation functions. Although we didn't find the exact expression for $\Delta_\xi(\omega)$ for these frequencies, it is qualitatively reproduced by the same functional form as in (16), but with $\phi(\omega) = \beta\ln(\omega/\bar{g})^2$, where $\beta = \beta_\xi$ scales as $\sqrt{\xi}$ at small ξ and saturates at $\beta \approx 0.38$ at large ξ. Replacing again ω by z and expressing z as $z = |z|e^{i\psi}$, we find after simple algebra that $\Delta_\xi(z)$ contains an additional set of poles at small z, but these poles are again located in the lower half-plane. At small ξ, the poles are at $|z_k| = \bar{g}e^{-k\pi/(2\beta)}$, $k = 1,\ 2\ldots$, along the directions when either ψ or $\pi - \psi$ equal $-\xi/(2\beta) \sim \xi^{1/2}$. These directions are close to the real axis, but still away from it. For large ξ, the expression for $|z_k|$ remains the same, but ψ increases and approaches $-\pi/2$, i.e., the poles move towards Matsubara axis.

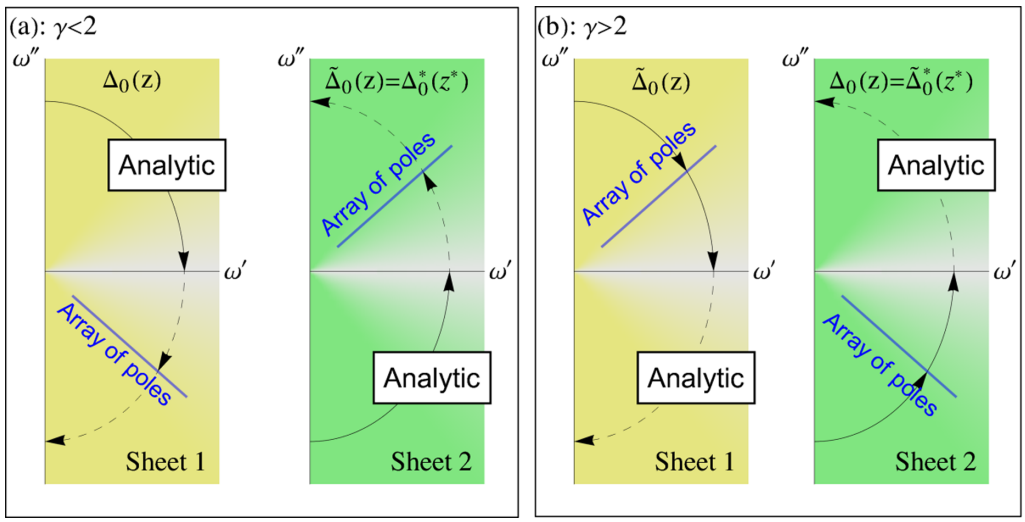

FIG. 17. An illustration of the analytical properties of the gap function $\Delta_0(z)$, when there is a line of poles in the complex plane. (a) $\gamma < 2$ The function $\Delta_0(z)$, obtained from $\Delta_0(\omega_m)$ by Pade approximants (sheet 1), is analytic in the upper half-plane and has poles in the lower half-plane, The function $\tilde{\Delta}_0(z) = [\Delta_0(z^*)]^*$ lives on the different sheet of the Riemann surface (sheet 2). It is analytic in the lower half-plane and has poles in the upper half-plane. Out of the two, $\Delta_0(z)$ on sheet 1 is the physical gap function. (b) $\gamma > 2$. Now Pade approximants (sheet 1) give $\tilde{\Delta}_0(z)$, which is analytic in the lower half-plane. In turn, the function $\Delta_0(z)$ from sheet 2 is analytic in the upper half-plane and is now the physical gap function.

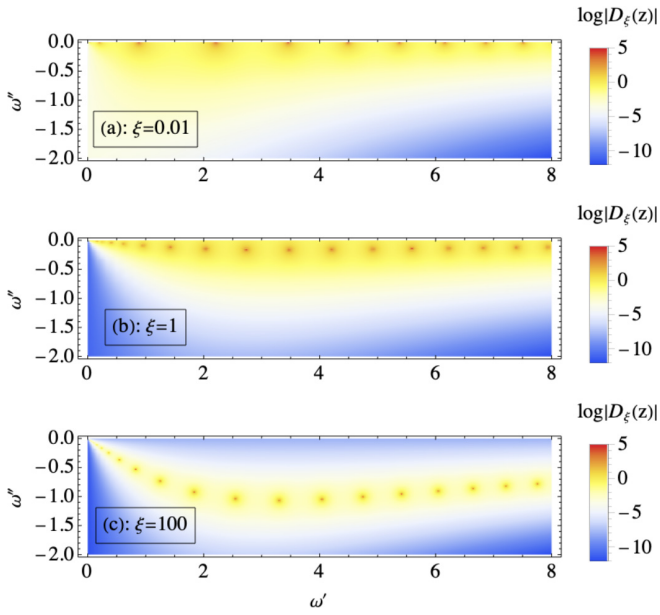

FIG. 18. The location of the poles of the gap function $\Delta_\xi(z)$ for $\xi = 0.01,\ 1,$ and 100. We extended Eq. (16) to complex z and for simplicity used the approximate interpolation form of the function $\phi(z)$: $\phi(z) = \beta \ln(z/\bar{g})^2 + z^2/(\pi\bar{g}^2)$, where $\beta = \beta_\xi$ scales as $\sqrt{\xi}$ at small ξ and saturates at $\beta \simeq 0.38$ at large ξ. The first and the second term in $\phi(z)$ determine the location of the poles at $|z| < \bar{g}$ and $|z| > \bar{g}$, respectively.

We note in passing that along the Matsubara axis, $\Delta_\xi(\omega_m)$ oscillates and contains nodes. At small ξ, the nodes are located at $|\omega_m| \sim \bar{g}e^{-(k-1/2)\pi/(2\beta)}$ with $k \in \mathbb{Z}$. At $\xi \to 0$, the nodes and the poles of $\Delta_\xi(z)$ approach $z = 0$, where they annihilate at $\xi = 0$, leaving a regular $\Delta_0(z)$ at small z. We illustrate this behavior in Fig. 19.

V. GAP EQUATION ALONG THE REAL FREQUENCY AXIS

We now address the issue of whether there are any qualitative differences in the behavior of observables at $T = 0$ between $\gamma < 2$ and $\gamma > 2$. In both cases, the condensation energy is the largest for the $n = 0$ solution, so we focus on the form of $\Delta_0(z)$. For definiteness, we consider the original γ model with $M = 1$. The behavior of the extended model with $M \neq 1$ is quite similar, as long as $M > 0$.

We found earlier in this paper that while the functional forms of $\Delta_0(z)$ are almost symmetric with respect to $\gamma - 2$, the gap functions $\Delta_0(z)$ at $\gamma < 2$ and $\gamma > 2$ live on different sheets of the Riemann surface.

We argue below that this topological distinction gives rise to a *qualitative* change in the behavior of the DOS, which at $\gamma > 2$ develops a nonintegrable singularity at the lower edge of the continuum. We show that this feature is robust against weak perturbations, in particular it survives when a pairing boson is massive, as long as the mass is below a certain finite threshold.

To demonstrate this, we analyze the form of the gap function $\Delta_0(\omega)$ at $\gamma > 2$. At the smallest and the largest frequencies, $\Delta_0(\omega)$ can be obtained by direct rotation from the Matsubara axis, i.e., by replacing $i\omega_m$ by $\omega + i0^+$. However, at intermediate $\omega \gtrsim \bar{g}$, which we will be interested in, this procedure is inadequate, as explained in Refs. [4–8], and one has to solve the full nonlinear gap equation (3), for which $\Delta_0(\omega_m)$ is an input. This equation, $\Delta(\omega)B(\omega) = A(\omega) + C(\omega)$, contains three functions of frequency, $A(\omega)$, $B(\omega)$, and $C(\omega)$. The functions $A(\omega)$ and $B(\omega)$ are expressed in terms of $\Delta_0(\omega_m)$ as

$$A(\omega) = \pi T \sum_{\omega_m > 0} \frac{D_0(\omega_m)}{\sqrt{1 + D_0^2(\omega_m)}} \times \left(\frac{\bar{g}^\gamma}{(\omega_m + i\omega)^\gamma} + \frac{\bar{g}^\gamma}{(\omega_m - i\omega)^\gamma} \right),$$
$$B(\omega) = 1 + \frac{i\pi}{\omega} T \sum_{\omega_m > 0} \frac{1}{\sqrt{1 + D_0^2(\omega_m)}} \times \left(\frac{\bar{g}^\gamma}{(\omega_m + i\omega)^\gamma} - \frac{\bar{g}^\gamma}{(\omega_m - i\omega)^\gamma} \right), \quad (18)$$

where, we remind, $D_0(\omega_m) = \Delta_0(\omega_m)/\omega_m$. Using the fact that $\Delta_0(\omega_m)$ is a monotonically decreasing function of frequency, one can make sure that at $\omega \gtrsim \bar{g}$, $A(\omega)$ and $B(\omega)$ are well approximated by $A(\omega) \simeq Q_{\gamma,0}(\bar{g}/|\omega|)^\gamma \cos\frac{\pi\gamma}{2}$, where $Q_{\gamma,0}$ is given by Eq. (9), and $B(\omega) \simeq 1$. The function $C(\omega)$ on the other hand is expressed in terms of the gap function in real

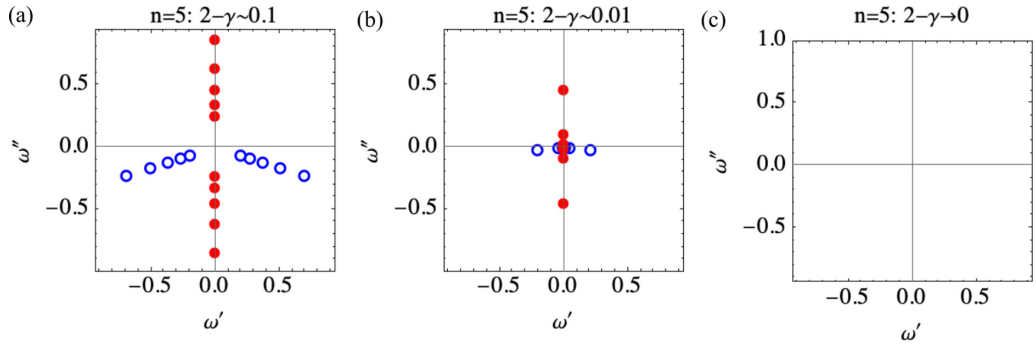

FIG. 19. A schematic plot of the location of zeros (solid circles) and poles (open circles) of $\Delta_n(z)$ with $n = 5$ near $z = 0$. A zero of $\Delta_n(z)$ gives rise to 2π anticlockwise variation of the phase of the gap function and in this respect acts as a vortex, and a pole of $\Delta_n(z)$ gives rise to -2π anticlockwise variation and acts as an antivortex. As $\gamma \to 2$, both vortices and anti-vortices move closer to $z = 0$. At $\gamma = 2$, they annihilate at $z = 0$, leaving a regular $\Delta_{\xi=0}(z)$ at small z.

frequencies as

$$C(\omega) = i\bar{g}^{\gamma} \sin\left(\frac{\pi\gamma}{2}\right) \int_{0^+}^{|\omega|} \frac{d\Omega}{\Omega^{\gamma}} \frac{D_0(|\omega|-\Omega) - D_0(|\omega|)}{\sqrt{1 - D_0^2(|\omega|-\Omega)}}. \tag{19}$$

The 0^+ in the lower limit of the integral in (19) implies that special care is needed to properly treat the limit $\Omega \to 0$, as the integrand in (19) is of order $1/\Omega^{\gamma-1}$ at small Ω, and $\int d\Omega/\Omega^{\gamma-1}$ is infrared divergent. The divergence is eliminated by slightly shifting the integration contour into the upper half-plane of frequency, as shown in Fig. 4 (see Appendix A for details). One can verify that this is equivalent to integrating in (19) along the real axis down to an infinitesimally small but finite ϵ and subtracting from the integral

$$\frac{-1}{\gamma-2} \frac{1}{\epsilon^{\gamma-2}} \frac{\frac{dD_0(\omega)}{d\omega}}{\sqrt{1 - D_0^2(\omega)}}. \tag{20}$$

The gap equation (3) is an integral equation on $\Delta_0(\omega)$. In papers IV and V, we converted this equation into the differential equation by Taylor expanding the integrand in (19). We use the same approach here. We follow Refs. [6,7] and express the gap function as $\Delta_0(\omega) = \omega/\sin\phi_0(\omega)$, where $\phi_0(\omega)$ is in general a complex function of frequency. At $\gamma = 2+0$, $C(\omega) = (\pi\bar{g}^2/2)\dot{\phi}_0/\sin\phi_0(\omega) = (\pi\bar{g}^2/2)\dot{\phi}_0 D_0(\omega)$. The equation on ϕ_0 then reduces to $\dot{\phi}_0 = (2/\pi\bar{g}^2)(\omega + Q_{2,0}(\bar{g}/\omega)^2 \sin\phi_0(\omega))$. The solution of this equation is a monotonically increasing *real* function $\phi_0(\omega)$ (Ref. [6]).

For $\gamma \neq 2$, the expansion of $C(\omega)$ in powers of $\dot{\phi}_0$ yields an infinite number of terms, all with prefactors $O(\gamma-2)$ at $\gamma \approx 2$. To get some physical insight, below we first follow paper IV and consider the toy model, in which keep only the first of these terms, the one with $\dot{\phi}_0^2$. Then we consider the actual gap equation and sum up series of terms with higher-order derivatives and higher powers of $\dot{\phi}_0$. We show that the structure of the gap function changes somewhat, compared with the toy model, but the outcome remains largely the same.

A. Expansion to order $\dot{\phi}_0^2(\omega)$

For convenience, we keep γ close to 2 and keep only terms linear in $2-\gamma$. Expanding in the integrand for $C(\omega)$ to order $\dot{\phi}_0^2$, we express the gap equation as

$$\dot{\phi}_0 + \omega\delta\dot{\phi}_0^2 \tan\phi_0 = \frac{2}{\pi\bar{g}^{\gamma}}\left(\omega^{\gamma-1} - Q_{\gamma,0}\frac{\bar{g}^{\gamma}}{\omega^2} e^{i\pi\gamma/2} \sin\phi_0\right), \tag{21}$$

where $\delta = (\gamma-2)/2$ and $\phi_0 = \phi_0(\omega)$.

We are interested in the behavior of $\phi_0(\omega)$ at $\omega \gtrsim \bar{g}$, where our approximations for $A(\omega)$ and $B(\omega)$ are valid. The initial condition for (21) can be set at some $\omega < \bar{g}$, where $\phi_0 < \pi/2$. Solving Eq. (21) at larger $\omega \gtrsim \bar{g}$, we find that $\phi_0(\omega)$ increases and remains real as long as it is smaller than $\pi/2$. In this range, $Q_{\gamma,0}$ is parametrically smaller than ω and can be safely neglected. Eq. (21) then becomes the quadratic equation on $\dot{\phi}_0$. Solving it and choosing the solution that matches the initial condition, we obtain

$$\dot{\phi}_0 = -\frac{1}{2\delta\omega\tan\phi_0}\left[1 - \sqrt{1 + \frac{8\delta\tan\phi_0}{\pi}\left(\frac{\omega}{\bar{g}}\right)^{\gamma}}\right]. \tag{22}$$

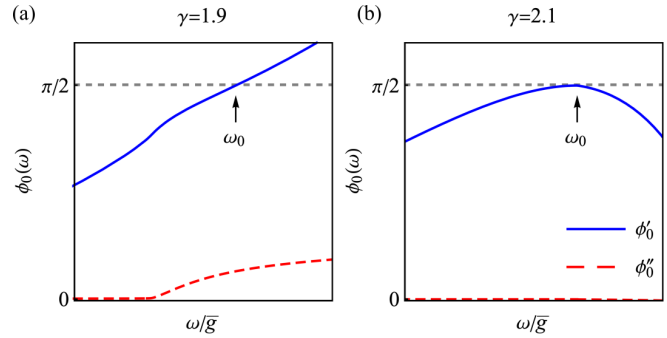

FIG. 20. The function $\phi_0(\omega)$ at $\omega \approx \omega_0$ for (a) $\gamma = 1.9$ and (b) 2.1, from the numerical solution of Eq. (21).

A simple analysis of this equation shows that the behavior of $\phi_0(\omega)$ at $\gamma < 2$ and at $\gamma > 2$ differ in one particular aspect. At $\gamma < 2$ (i.e., $\delta < 0$), the imaginary part of $\phi_0(\omega)$ emerges at $(8/\pi)|\delta|\tan\phi_0(\omega/\bar{g})^{\gamma} = 1$, before ϕ_0 reaches $\pi/2$. A straightforward analysis of Eq. (22) shows that at larger ω, $\phi_0(\omega)$ becomes complex, and both $\phi'(\omega)$ and $\phi''(\omega)$ are positive and increase with frequency as $\omega^{\gamma/2}$. At even larger ω, the $Q_{\gamma,0}$ term in (21) becomes relevant. At these ω, $\phi'(\omega)$ saturates and $\phi''(\omega)$ keep increasing, but logarithmically. The high-frequency behavior yields $\Delta_0(\omega) \propto 1/\omega^{\gamma}$, consistent with the fact that at large frequencies the transformation from $\Delta_0(\omega_m)$ to $\Delta_0(\omega)$ is a simple rotation.

For $\gamma > 2(\delta > 0)$, the solution changes. Now ϕ_0 remains real up to a frequency, ω_0, where $\phi_0 = \pi/2$ and $\tan\phi_0$ diverges. An elementary analysis of (22) shows that $\dot{\phi}_0$ vanishes upon approaching this point and

$$\phi_0 = \frac{\pi}{2} - \frac{1}{2\pi\delta}\frac{\omega_0^{\gamma-2}}{\bar{g}^{\gamma}}(\omega-\omega_0)^2 - \frac{1}{8\pi\delta^2}\frac{\omega_0^{\gamma-3}}{\bar{g}^{\gamma}}(\omega-\omega_0)^3 + \ldots. \tag{23}$$

At larger $\omega > \omega_0$, Eq. (22) does not have a solution. To obtain $\phi_0(\omega)$ at such ω, one has to choose another solution of the quadratic equation on $\dot{\phi}_0$

$$\dot{\phi}_0 = -\frac{1}{2\delta\omega\tan\phi_0}\left[1 + \sqrt{1 + \frac{8\delta\tan\phi_0}{\pi}\left(\frac{\omega}{\bar{g}}\right)^{\gamma}}\right], \tag{24}$$

which implies that $\Delta_0(\omega)$ moves to a different sheet of the Riemann surface.

Solving (24) we find that at $\omega \gtrsim \omega_0$, $\phi_0(\omega)$ remains real and is still given by Eq. (23). We verified this result by solving the full Eq. (21) numerically. In Fig. 20, we show the numerical results for $\gamma = 1.9$ and 2.1. We see that, at $\gamma = 1.9$, Re $\phi_0(\omega)$ increases monotonically and Im $\phi_0(\omega)$ emerges before Re $\phi_0(\omega)$ reaches $\pi/2$. At $\gamma = 2.1$, $\phi_0(\omega)$ remains real and varies quadratically near ω_0, where $\phi_0(\omega_0) = \pi/2$.

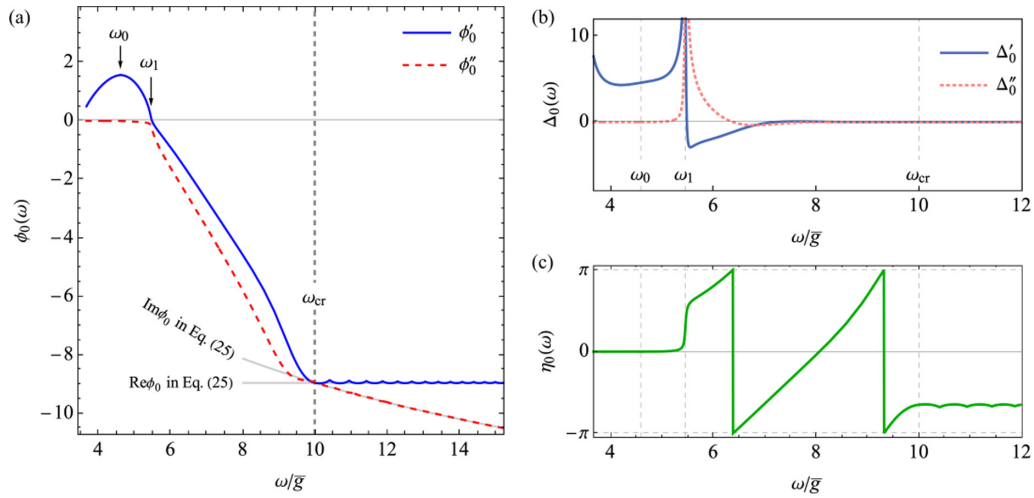

FIG. 21. (a) Solution of full differential equation Eq. (21) with the $Q_{0,\gamma}$ term included, at $\gamma = 2.7$. Gray lines show asymptotic behavior at large frequencies, consistent with Eq. (26). (b) The real and the imaginary parts of the gap function $\Delta_0(\omega) = \omega/\sin\phi_0(\omega)$. (c) The phase $\eta_0(\omega) = \mathrm{Arg}[\Delta_0(\omega)]$.

The function $\phi_0(\omega)$ remains real up to frequency $\omega_1 > \omega_0$, at which it reduces down to $\phi_0 = 0$. At around this frequency,

$$\phi_0 \simeq \sqrt{\frac{2}{\delta\omega_1}(\omega_1 - \omega - i0^+)} + \frac{4}{3\pi}\frac{\omega_1^{\gamma-1}}{\bar{g}^\gamma}(\omega_1 - \omega) + \ldots \tag{25}$$

When ω exceeds ω_1, a negative ϕ_0'' emerges and gradually increases in amplitude. The real part ϕ_0' also becomes negative. At larger frequencies $\phi_0' \sim \phi_0'' \sim -\omega^{\gamma/2}/\sqrt{\pi\delta\bar{g}^\gamma}$. We verified this behavior by solving Eq. (24) numerically, see Fig. 21(a). We clearly see that $\phi_0''(\omega)$ emerges at $\omega = \omega_1$ and both ϕ_0' and ϕ_0'' scale as $\omega^{\gamma/2}$ at larger ω. As $|\phi_0''|$ increases, $\sin\phi_0$ also increases, and above a certain frequency the $Q_{\gamma,0}$ term in the right-hand side (r.h.s.) of Eq. (21) cannot be neglected. At even larger frequencies, the two terms balance each other, and we obtain

$$\phi_0' = -2m\pi - (\gamma - 1)\frac{\pi}{2},$$
$$\phi_0'' = -\ln\frac{2\bar{g}}{Q_{0,\gamma}} - (1+\gamma)\ln\frac{\omega}{\bar{g}}. \tag{26}$$

where m is the number of vortices in the first quadrant ($m = 2$ for particular $\gamma = 2.7$ in Fig. 21). This yields $\Delta_0(\omega) \propto 1/\omega^\gamma$ at the largest frequencies, as it should be.

We plot $\mathrm{Re}\Delta_0(\omega)$ and $\mathrm{Im}\Delta_0(\omega)$ in Fig. 21(b) and the phase $\eta_0(\omega)$ of $\Delta_0(\omega) = |\Delta_0(\omega)|e^{i\eta_0(\omega)}$ in Fig. 21(c). The phase undergoes two slips by 2π at positive ω, consistent with the existence of two vortices on the upper half-plane of frequency.

1. Density of states

The density of single-electron states is defined as $N(\omega) = (-N_0/\pi)\mathrm{Im}G_l(\omega)$, where N_0 is the DOS in the normal state and $G_l(\omega)$ is the (retarded) local single-electron Green's function. To be specific, we consider the case of dispersion-full fermions with pairing mediated by a massless collective bosonic excitation. In this case, the local Green's function is obtained by integrating over momentum transverse to the Fermi surface. In the Eliashberg theory, which assumes that fermionic bandwidth is the largest scale in the problem, the momentum integration is converted into the integration over fermionic dispersion ϵ_k near the Fermi surface and is approximated by $(2\pi)^{-d}\int d^dk = N_0\int d\epsilon_k$, where d is the spatial dimensionality of the system, and extends to infinite limits. Then

$$G_l(\omega) = -i\pi\sqrt{\frac{\omega^2}{\omega^2 - \Delta_0^2(\omega)}}, \tag{27}$$

In terms of $\phi_0(\omega)$, $N(\omega) = N_0\mathrm{Re}\sqrt{-\tan^2\phi_0}$.

One can easily verify that the DOS vanishes at small frequencies, as expected for a superconductor with a finite gap, and is nonzero at frequencies $\omega > \omega_1$, where Im $\phi_0(\omega)$ is finite. It is tempting to call ω_1 a spectral gap, by analogy with a BCS/Eliashberg superconductor. For $\gamma < 2$, there are no other features in the DOS, although there is a structure inside the continuum. For $\gamma > 2$, there is also a continuum above ω_1, but in addition, there appears a bound state inside the gap, at $\omega = \omega_0 < \omega_1$. At this frequency $\tan\phi_0$ diverges and a nonzero $N(\omega)$ emerges once we shift ω into the upper frequency half-plane by an infinitesimally small amount. Moreover, because $N(\omega) \sim \mathrm{Im}[1/(\omega - \omega_0 + i0)^2]$, the integral of the DOS over an infinitesimally narrow range around ω_0 diverges. The prefactor for the divergent term (the capacity of the level) scales as $\delta = \gamma - 2$. For a lattice system with a finite total number of states, the total weight of the bound state is finite, but is a function of the total number of states per unit volume, i.e., the bound state is macroscopically degenerate.

We show the result of numerical evaluation of the DOS for representative $\gamma = 2.1$ in Fig. 22. We clearly see that the DOS has a continuum, which starts at ω_1, and an in-gap bound state at $\omega_0 < \omega_1$. The weight of the bound state is comparable to the total weight of the continuum.

B. Equation for $\phi_0(\omega)$ with derivatives to all orders

We now analyze the full equation for $\phi_0(\omega)$, with infinite series of higher-order derivatives in the left-hand side (l.h.s.).

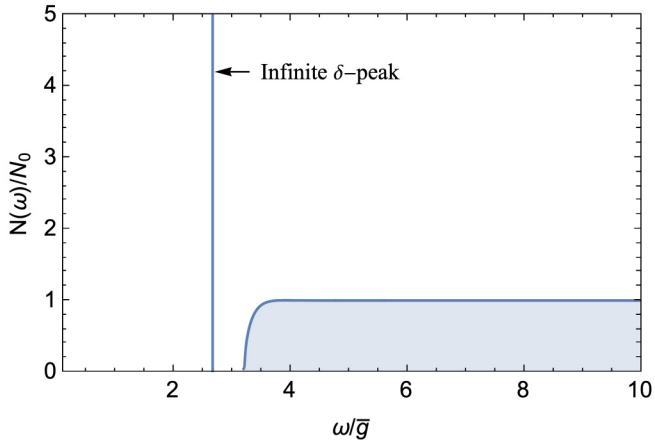

FIG. 22. The density of states $N(\omega)$ for $\phi(\omega)$ determined by Eq. (21). We set $\gamma = 2.1$.

These derivatives appear in combination with higher powers of $\tan\phi_0$, which diverges at $\omega = \omega_0$, hence it is a'priori unclear whether the bound state with a macroscopic degeneracy survives. We show below that it does survive.

The analysis is rather involved and we present the details in Appendix C. There are two types of terms in the expansion of $C(\omega)$ in the derivatives of $\phi_0(\omega)$: terms with higher powers of $\dot\phi_0$, combined with higher powers of $\tan\phi_0$, and terms with higher derivatives of ϕ_0, see Eq. (C2). We argue in Appendix C that the terms with higher derivatives are irrelevant, but the terms with higher powers of $\dot\phi_0$ must be kept. These last terms form series in $X = \omega\dot\phi_0\tan\phi_0$ in the form

$$C(\omega) = \frac{\bar g^\gamma}{\omega^{\gamma-2}}\frac{\sin\frac{\pi\gamma}{2}}{2-\gamma}D(\omega)\dot\phi_0\Big[1+\frac{\gamma-2}{2(3-\gamma)}X-\frac{\gamma-2}{2(4-\gamma)}X^2 +\frac{\gamma-2}{2(5-\gamma)}X^3+\dots\Big]. \tag{28}$$

The series in Eq. (28) sum up into hypergeometric function ${}_2F_1(1,2-\gamma,3-\gamma,-X)$. Substituting into the gap equation and again neglecting the $Q_{\gamma,0}$ term, we obtain the differential equation on $\phi_0(\omega)$ in the form

$$\frac{1}{2}\dot\phi_0[1+{}_2F_1(1,2-\gamma,3-\gamma,-X)] = \frac{2}{\pi\bar g^\gamma}\omega^{\gamma-1}. \tag{29}$$

This equation is valid as long as X remains positive, i.e., as long as $\phi_0 < \pi/2$. We assume and then verify that $\phi_0(\omega)$ increases with ω and remains real up to a frequency ω_0, at which it reaches $\pi/2$. At $\omega \lesssim \omega_0$, X is large and the asymptotic expansion of a Hypergeometric function yields ${}_2F_1(1,2-\gamma,3-\gamma,-X) \approx X^{\gamma-2}\Gamma(3-\gamma)\Gamma(\gamma-1)$. Substituting into (29) and solving for $\phi_0(\omega)$ near ω_0, we obtain

$$\phi_0(\omega) \simeq \frac{\pi}{2} - \frac{4}{\pi}\Big(\frac{\omega_0}{\bar g}\Big)^\gamma \frac{B_\gamma(1-\omega/\omega_0)^{\gamma-1}}{1+B_\gamma(1-\omega/\omega_0)^{\gamma-2}}, \tag{30}$$

$$B_\gamma = \frac{1}{(\gamma-1)^{\gamma-1}\Gamma(3-\gamma)\Gamma(\gamma-1)}. \tag{31}$$

For $\gamma < 2$, this yields

$$\phi_0(\omega) \simeq \frac{\pi}{2} - \frac{4}{\pi}\Big(\frac{\omega_0}{\bar g}\Big)^\gamma\Big(\Big(1-\frac{\omega}{\omega_0}\Big) -\frac{1}{\bar B_\gamma}\Big(1-\frac{\omega}{\omega_0}\Big)^{3-\gamma}+\dots\Big), \tag{32}$$

where $\bar B_\gamma = \frac{3-\gamma}{\Gamma(3-\gamma)\Gamma(\gamma-1)}$.

The derivative $\dot\phi_0$ remains finite and positive at $\omega = \omega_0$. It is then natural to expect that $\phi'(\omega)$ continue increasing at $\omega > \omega_0$, i.e., X jumps from $+\infty$ to $-\infty$. Simultaneously $\phi_0''(\omega)$ becomes nonzero due to subleading term in (32). There is an ambiguity about the sign of $\phi_0''(\omega)$ as the Hypergeometric function ${}_2F_1(1,2-\gamma,3-\gamma,-X)$ has a branch cut along $X \in (-\infty,-1]$. Extending X to $X \pm i0$ [equivalent to shifting ω to $\omega \pm i0$ in Eq. (30)], leads to two conjugate solutions, which reside on different sheets of the Riemann surface of ${}_2F_1(1,2-\gamma,3-\gamma,-X)$. The correct sheet has to be chosen to preserve the analyticity of $\Delta_0(\omega) = \omega/\sin\phi_0(\omega)$ in the upper half-plane. A simple analysis shows for this $\phi_0''(\omega)$ must be positive near ω_0. For $\gamma < 2$, we verified that analysis shows that the natural extension ω to $\omega \to \omega + i0$ is the correct one. Using it, we obtain at $\omega \geqslant \omega_0$,

$$\phi_0'(\omega) \approx \frac{\pi}{2} + \frac{4}{\pi}\Big(\frac{\omega_0}{\bar g}\Big)^\gamma\Big(\frac{\omega}{\omega_0}-1\Big),$$

$$\phi_0''(\omega) \approx \frac{4}{\pi\bar B_\gamma}\Big(\frac{\omega_0}{\bar g}\Big)^\gamma \sin[\pi(2-\gamma)]\Big(\frac{\omega}{\omega_0}-1\Big)^{3-\gamma}. \tag{33}$$

We see that indeed $\phi''(\omega) > 0$.

For $\gamma > 2$, we have at $\omega < \omega_0$

$$\phi_0(\omega) \simeq \frac{\pi}{2} - \frac{4}{\pi}B_\gamma\Big(\frac{\omega_0}{\bar g}\Big)^\gamma\Big(\Big(1-\frac{\omega}{\omega_0}\Big)^{\gamma-1} -B_\gamma\Big(1-\frac{\omega}{\omega_0}\Big)^{2\gamma-3}+\dots\Big). \tag{34}$$

For $\omega > \omega_0$, a simple experimentation shows that, to preserve analyticity, we need to extend $\omega \to \omega - i0$, i.e., choose the solution on a different sheet of the Riemann surface. We then obtain

$$\phi_0'(\omega) \approx \frac{\pi}{2} + \frac{4}{\pi}B_\gamma\Big(\frac{\omega_0}{\bar g}\Big)^\gamma \cos[\pi(\gamma-2)]\Big(\frac{\omega}{\omega_0}-1\Big)^{\gamma-1}, \tag{35}$$

$$\phi_0''(\omega) \approx \frac{4}{\pi}B_\gamma\Big(\frac{\omega_0}{\bar g}\Big)^\gamma \sin[\pi(\gamma-2)]\Big(\frac{\omega}{\omega_0}-1\Big)^{\gamma-1}. \tag{36}$$

Then

$$D_0(\omega) = \frac{1}{\sin\phi_0(\omega)} = 1 + A\Big(\frac{\omega_0-\omega+i0}{\omega_0}\Big)^{2(\gamma-1)}, \tag{37}$$

where A is positive and $O(1)$. This is rather similar to the situation for the toy model. The new element is that now $\phi_0''(\omega)$ develops immediately above ω_0, i.e., there is no frequency range where $\phi_0(\omega)$ bends down. We show the numerical solution of Eq. (29) in Fig. 23.

1. Density of states

We see from (37) that for $\gamma > 2$, $D_0(\omega)$ approaches 1 at $\omega = \omega_0$ with zero derivative. This is similar to the behavior of

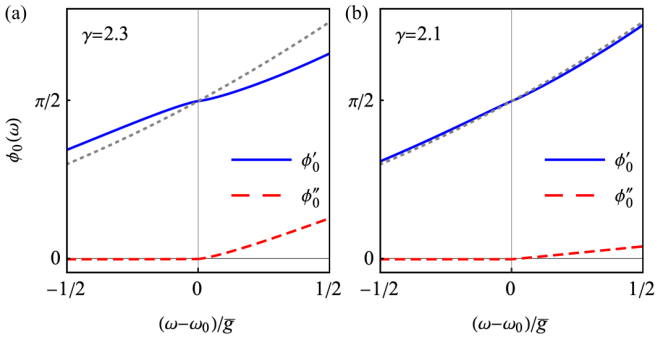

FIG. 23. Solution of the modified gap equation Eq. (29) around ω_0, where (a) $\gamma = 2.3$ and (b) $\gamma = 2.1$. Gray dotted line shows the solution at $\gamma = 2$: $\phi_0(\omega) = \omega^2/\pi$.

ϕ_0 in the toy model, although the exponent remains smaller than 2 for all $\gamma < 3$. We now show that the vanishing of the derivative gives rise to a nonintegrable singularity in the DOS at $\omega = \omega_0$. Indeed, near $\omega = \omega_0$, the DOS has the form

$$\frac{N(\omega)}{N_0} = \frac{\bar{g}^\gamma}{\omega_0}\frac{\pi\sin(\pi(\gamma-2))}{4B_\gamma}\frac{\Theta(\omega-\omega_0)}{(\omega-\omega_0)^{\gamma-1}}, \tag{38}$$

where $\Theta(x)$ is the unit step function. In distinction from the toy model, the continuum in the DOS is present for all $\omega > \omega_0$. Still, $\int_{\omega_0}^{\infty} d\omega N(\omega)$ diverges at the lower limit, i.e., the DOS contains a nonintegrable singularity at $\omega = \omega_0 + 0$. As we said, for a lattice system this implies that the number of states within a tiny interval above ω_0 is some function of the total number of states per unit volume. Because $N(\omega) \propto (\gamma - 2)$, the fraction initially increases linearly with $\gamma - 2$.

We show the DOS for several γ in Fig. 24. We see that the DOS vanishes below ω_0, forms a continuum above this frequency, and displays a sharp edge singularity with the weight comparable to the total weight of the continuum.

We note in passing that for smaller γ between 1 and 2 the DOS still diverges at $\omega = \omega_0 + 0$ with the fractional exponent $\gamma - 1$, but the singularity is now integrable, like in a BCS superconductor. We also note that for $\gamma \neq 2$, the pole of the Green's function yields dispersing excitations with $\omega - \omega_0 \propto e^{i\pi/2(\gamma-1)}|\bar{\xi}|^{1/(\gamma-1)}$, where $\bar{\xi}$ is the fermionic dispersion ($\int d^dk/(2\pi)^d = N_0\int d\bar{\xi}$). One can easily make sure that the edge singularity at $\gamma > 2$ is related to the fact that the exponent $1/(\gamma-1) < 1$. For $\gamma = 2$, we have $\omega - \omega_p \propto i|\bar{\xi}|$, where ω_p is the position of the peak in the DOS. In this situation, the spectral function near ω_p remains peaked at exactly $\omega = \omega_p$ even at a finite $\bar{\xi}$. This is consistent the DOS consisting of discrete levels.

2. *Continuity at $\gamma = 2 + 0$*

We see from Eq. (30) that at $\gamma = 2 + 0$, the frequency dependence of $\phi_0(\omega)$ becomes ω^2/π (which corresponds to taking $\gamma \to 2$ keeping ω away from ω_0), like at $\gamma = 2$ (see Refs. [5–7]). We show the numerical solution of Eq. (29) in Fig. 23. We see that the behavior of $\phi_0(\omega)$ at $\gamma > 2$ continuously approaches that at $\gamma = 2$: Im $\phi_0(\omega)$ gradually gets smaller and Re $\phi_0(\omega)$ approaches ω^2/π. Simultaneously, the maxima in the continuum in the DOS get sharper and at $\gamma = 2 + 0$ evolve into a discrete set of δ-functional peaks, see Fig. 24. We emphasize that the continuity at $\gamma \to 2$ does not hold in our approximate treatment in the previous subsection and emerges only after we sum up infinite series in $\dot{\phi}_0 \tan\phi_0$.

On a more closer look, we find that the analysis at $\gamma \to 2 + 0$ needs extra care. In this limit, the series in X yields to first order in δ

$$\begin{aligned} C(\omega) &= \frac{\pi\bar{g}^\gamma}{2\omega^{\gamma-2}}D(\omega)\dot{\phi}_0\left[1+\delta\left(X-\frac{X^2}{2}+\frac{X^3}{3}+\ldots\right)\right] \\ &= \frac{\pi\bar{g}^\gamma}{2\omega^{\gamma-2}}D(\omega)\dot{\phi}_0[1+\delta\ln(1+X)], \end{aligned} \tag{39}$$

where, we remind, $\delta = (\gamma-2)/2$. Substituting into the gap equation and restricting to $\omega \sim \omega_0$, we obtain

$$\dot{\phi}_0[1+\delta\ln(1+\omega\dot{\phi}_0\tan\phi_0)] = \frac{2}{\pi\bar{g}^\gamma}\omega^{\gamma-1}. \tag{40}$$

Solving this equation, we find that $\phi_0(\omega) \approx (2/\pi\gamma)(\omega/\bar{g})^\gamma$ up to an exponentially short distance to ω_0, and within this distance

$$\phi_0(\omega) \simeq \frac{\pi}{2} + \frac{2}{\pi\delta}\left(\frac{\omega_0}{\bar{g}}\right)^2\frac{1-\omega/\omega_0}{\ln(1-\omega/\omega_0-i0^+)}. \tag{41}$$

We see that $\phi_0(\omega)$ still approaches $\pi/2$ with zero derivative, but vanishes only logarithmically. The Im $\phi_0(\omega)$ does develop immediately above ω_0 like at larger γ, but in the immediate

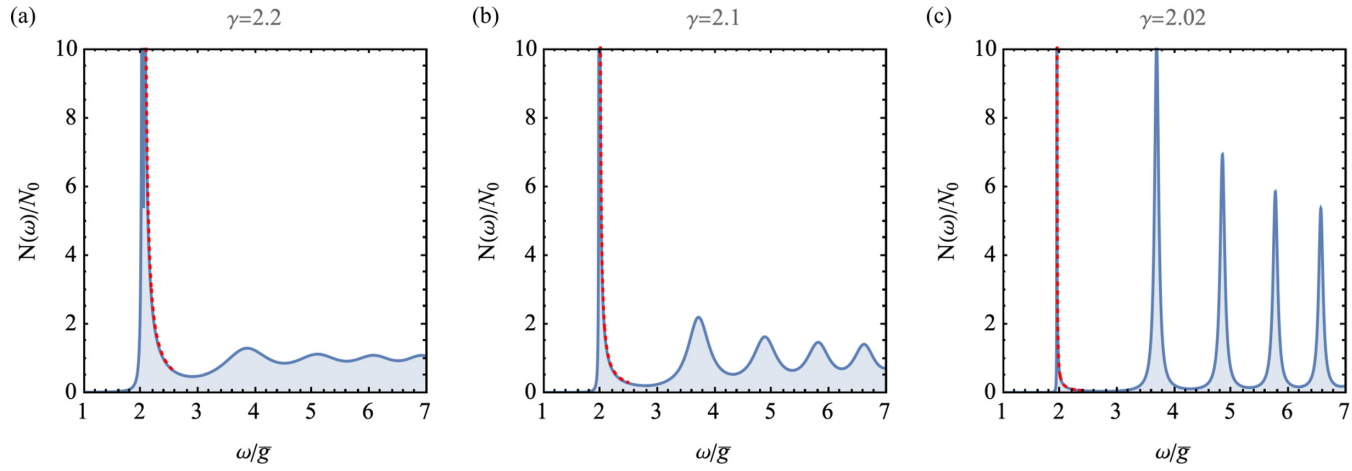

FIG. 24. Evolution of DOS, obtained by solving Eq. (29) for different γ, approaching $\gamma = 2$ from above. The red dotted line is the analytic result, Eq. (38).

vicinity of ω_0, Im $\phi_0(\omega)$ is parametrically small compared to Reϕ_0 by $1/|\ln(\omega-\omega_0)$. If we were to neglect Im $\phi_0(\omega)$, we would find that Re $\phi_0(\omega)$ monotonically increases with ω, as $(\omega/\bar{g})^2/\pi$, and just flattens in exponentially small regions near the frequencies where $\phi_0(\omega)=\pi/2+p\pi$.

Finally, we consider the terms with higher derivatives, like $\ddot{\phi}_0$, $\dddot{\phi}_0$, etc. For definiteness, let's restrict to $\gamma \geqslant 2$ and compare these terms with $(\gamma-2)\dot{\phi}\ln X$. Each term with a higher derivative gets renormalized by series in X. We evaluate the series in Appendix C. At large X, which we are interested in, the series for each term have the same asymptotic form and reduce each prefactor by $1/2$. Including these terms with rescaled prefactors, we find that the last term in Eq. (39) changes to

$$1+\delta[\ln(1+X)+K], \tag{42}$$

where

$$K=\frac{\omega}{\phi_0^{(1)}}\left(\frac{1}{2!}\phi_0^{(2)}-\frac{\omega}{3!2}\phi_0^{(3)}+\frac{\omega^2}{4!3}\phi_0^{(4)}+\ldots\right), \tag{43}$$

where $\phi_0^{(m)}$ is the m-th derivative of $\phi_0(\omega)$. We assume and then verify that at large X, i.e., at $\omega\approx\omega_0$, the inclusion of the K term only changes the prefactor for the second term in Eq. (41). To see this, we assume that at ω slightly below ω_0, $\phi_0(\omega)=\pi/2+Q(\omega_0-\omega)/\ln(1-\omega/\omega_0)$ with $Q=4\omega_0^{\gamma-1}/[\pi(\gamma-2)\bar{g}^\gamma]$, and compute the series for K using this form of ϕ_0. A straightforward analysis then yields

$$K=-\frac{1}{2\ln X}F(X), \tag{44}$$

where

$$\begin{aligned}F(X)&=2X\sum_{m=0}^{\infty}\frac{(-1)^m X^m}{(m+1)^2(m+2)}\\&=-2(\mathrm{Li}_2(-X)+\ln(1+X)(1+1/X)-1)\end{aligned} \tag{45}$$

and $\mathrm{Li}_2(-X)$ is a polylogarithm. At large X, $\mathrm{Li}_2(-X)\approx(-1/2)\ln^2 X$. Substituting into Eq. (44), we obtain $K\approx-(1/2)\ln X$. Substituting into Eq. (42), we see that the $\ln X$ dependence survives, only the prefactor drops by a factor of 2. Then Eq. (41) remains valid, with extra 2 in the prefactor for the second term. At the largest X, for which $\delta\ln X\gg 1$, the analysis requires more care. We verified that the end result remains the same terms with higher derivatives do not change qualitatively the expression for $\phi(\omega)$.

C. Extraction of the nonintegrable singularity in the DOS directly from the integral gap equation

We next show that the nonintegrable singularity in the DOS can be obtained directly from the integral equation (3). For this, we first rewrite this equation in the form, which takes care of the regularization of the formal divergence of the integral for $C(\omega)$ in Eq. (19):

$$\begin{aligned}\Delta(\omega)=\frac{1}{2}\int\frac{d\omega_m}{(-(i\omega_m-\omega)^2)^{\gamma/2}}\frac{\Delta(\omega_m)-\Delta(\omega)\frac{i\omega_m}{\omega}}{\sqrt{{\omega_m}^2+\Delta^2(\omega_m)}}\\+\frac{\sin(\pi\gamma/2)}{\gamma-2}\left(\dot{D}(\omega)\int_0^\omega\frac{\dot{g}(\Omega)d\Omega}{(\omega-\Omega)^{\gamma-2}}-(2-\gamma)\right.\\\left.\times\int_0^\omega d\Omega\frac{D(\Omega)-D(\omega)+(\omega-\Omega)\dot{D}(\omega)}{(\omega-\Omega)^\gamma}g(\Omega)\right),\end{aligned} \tag{46}$$

where

$$g(\omega)=\frac{1}{\sqrt{D^2(\omega)-1}}. \tag{47}$$

We take as an input the evidence from the numerical analysis that at small ω, $\Delta(\omega)$ is real, and that there exists ω_0, at which $\Delta(\omega_0)=\omega_0$. At this point, we have

$$\Delta(\omega_0)=\omega_0,\quad D(\omega_0)=1.$$

Let's assume that for ω just below ω_0 we have

$$D(\omega)=1+A(\omega_0-\omega)^\alpha,\quad \alpha>0,$$

where A is some real positive constant.

The integral over ω_m in Eq. (46) is completely regular at $\omega\to\omega_0$, the dangerous terms are the ones coming from the upper limit of integration over Ω in the last term. We then write $\omega=\omega_0-\epsilon_\omega$, and $\Omega=\omega_0-\epsilon_\omega-\epsilon_\Omega$, assume that both ϵ_ω and ϵ_Ω are small, and consider the contribution from the upper limit. Then

$$\begin{aligned}g(\Omega)&\approx\frac{1}{\sqrt{2A}}\frac{1}{(\epsilon_\omega+\epsilon_\Omega)^{\alpha/2}},\\g'(\Omega)&\approx\frac{\alpha}{2}\frac{1}{\sqrt{2A}}\frac{1}{(\epsilon_\omega+\epsilon_\Omega)^{\alpha/2+1}}.\end{aligned} \tag{48}$$

Expressing $\epsilon_\Omega=x\epsilon_\omega$, we then obtain the dangerous contribution to the gap equation in the form

$$\begin{aligned}\epsilon_\omega^{1+\alpha/2-\gamma}\frac{\sqrt{A}}{\sqrt{2}}\left(\frac{\alpha^2}{2}\int_0\frac{dx}{x^{\gamma-2}}\frac{1}{(1+x)^{\alpha/2+1}}\right.\\\left.-(2-\gamma)\int_0 dx\frac{(1+x)^\alpha-1+x\alpha}{x^\gamma(1+x)^{\alpha/2}}\right).\end{aligned}$$

In order for this term to be finite, we must have

$$\alpha\geqslant 2(\gamma-1)>2.$$

By continuity, we expect $\alpha=2$ at $\gamma=2$ (see previous section). Invoking this argument, we find $\alpha=2(\gamma-1)$. This is exactly the same form as we obtained by summing up Taylor series, Eq. (37).

The function $g(\Omega)$ must be analytic in the upper half plane. For the same reasoning as above, for $\gamma>2$ this requires changing ω to $\omega-i0$. Substituting $\epsilon_\omega+\epsilon_\Omega=\omega_0-\Omega+i0$ into Eq. (48), we obtain

$$g(\Omega)\approx\frac{1}{\sqrt{2A}}\frac{1}{(\omega_0-\Omega+i0)^{\gamma-1}}.$$

The imaginary part of g is proportional to the density of states. We have

$$\begin{aligned}N(\Omega)&\propto\frac{1}{\sqrt{2A}}\mathrm{Im}\frac{1}{(\omega_0-\Omega+i0)^{\gamma-1}}\\&=\begin{cases}0, & \text{if } \Omega<\omega_0\\ \frac{1}{\sqrt{2A}}\frac{\sin(\pi(1-\gamma))}{(\Omega-\omega_0)^{\gamma-1}}, & \text{if } \Omega>\omega_0\end{cases}.\end{aligned}$$

This is the same expression as Eq. (38).

VI. FINITE ω_D

In this section, we examine whether the state with an "infinite" peak in the DOS is stable with respect to perturbation imposed by a small but finite mass of the pairing boson. On the Matsubara axis, a finite mass of the boson changes the interaction to

$$V(\Omega_m) = \frac{\bar{g}^\gamma}{\left[\Omega_m^2 + \omega_D^2\right]^{\gamma/2}}. \tag{49}$$

A finite ω_D eliminates the solutions with large n, leaving only a finite number of the gap functions. The number of remaining solutions decreases as ω_D increases, and beyond some threshold only the $n = 0$ solution survives. At the same time, the form of $\Delta_0(\omega_m)$ is only weakly affected by ω_D both for $\gamma < 2$ and $\gamma > 2$.

On the real axis, the effect of ω_D on the $n = 0$ solution is stronger, but we show that the edge singularity survives as long as ω_D remains below some finite threshold. To demonstrate this, we analyze how a finite ω_D affects the gap on the real axis.

One can easily verify that the terms $B(\omega)$ and $A(\omega)$ in the gap equation $D(\omega)B(\omega) = A(\omega) + C(\omega)$, are only weakly affected by ω_D, as long as ω_D remains much smaller than $\bar{g}$ and can be safely kept the same as at $\omega_D = 0$. The key effect of a finite ω_D is on the term $C(\omega)$. We analyze this effect in two steps, like in Sec. V. Namely, we first keep only the $\dot{\phi}_0^2 \tan\phi_0$ term in the expansion of $C(\omega)$ in the derivatives of $\phi_0(\omega)$, and then include the series of higher-order terms. The equation on $\phi_0(\omega)$ to order $\dot{\phi}_0^2 \tan\phi_0$ in the presence of ω_D has been derived in paper V for $\gamma = 2$. Combining it with Eq. (21), we obtain

$$\dot{\phi}_0 + \dot{\phi}_0^2 \tan\phi_0 \times \left(\frac{\gamma-2}{2}\omega - \frac{\gamma}{4}\omega_D\right) = \frac{2}{\pi\bar{g}^\gamma}\left(\omega^{\gamma-1} - Q_{\gamma,0}\frac{\bar{g}^\gamma}{\omega^2}e^{i\pi\gamma/2}\sin\phi_0\right), \tag{50}$$

As before, we will be interested in $\omega \approx \omega_0$, where $\phi_0(\omega)$ reaches $\pi/2$, and neglect the $Q_{\gamma,0}$ term.

We see from Eq. (50) that the two terms in the prefactor for $\dot{\phi}_0^2 \tan\phi_0$ have opposite signs and hence compete. To analyze the competition, we the introduce

$$\omega_c = \frac{\gamma}{2(\gamma-2)}\omega_D. \tag{51}$$

Solving Eq. (50) for $\dot{\phi}_0$ at frequencies where $\tan\phi_0 > 0$ and choosing the solution which matches the initial condition at $\omega \lesssim \bar{g}$, we obtain

$$\dot{\phi}_0 = \frac{-1 + \sqrt{1 + \frac{8\delta_{\rm eff}}{\pi}\omega^\gamma \tan\phi_0}}{2\delta_{\rm eff}\omega\tan\phi_0}. \tag{52}$$

This is the same equation as (22), but with

$$\delta_{\rm eff} = \frac{\gamma-2}{2}\left(1 - \frac{\omega_c}{\omega}\right) = \frac{\gamma\omega_D}{4\omega_c}\left(1 - \frac{\omega_c}{\omega}\right). \tag{53}$$

For small ω_D and $\gamma - 2$, relevant ω is near $\omega_0 \approx \bar{g}\pi/\sqrt{2}$, where $\phi_0 = \pi/2$ at $\gamma = 2$ and $\omega_D = 0$. Then $\delta_{\rm eff} \approx (\omega_D/(2\omega_0))(\gamma - 2 - \omega_D/\omega_0)$. We see that ω_D effectively shifts the critical value of the topological transition from $\gamma = 2$ to $\gamma_D = 2 + \omega_D/\omega_0$. When $2 < \gamma < \gamma_D$, or, equivalently, $\omega_D > (\gamma-2)\omega_0$, $\phi_0''(\omega)$ emerges before ϕ_0' reaches $\pi/2$, and the DOS has only a continuum above the spectral gap. When $\gamma > \gamma_D$, or, equivalently, $\omega_D < (\gamma-2)\omega_0$, $\phi_0(\omega)$ remains real up to ω_0, and then moves to a different sheet of the Riemann surface. In this situation, the DOS has a continuum and a macroscopically degenerate bound state below the continuum. We show this behavior in Fig. 25. We emphasize that there is a single line of a topological transition in the (ω_D, γ) plane, i.e., once the gap function moves to a different sheet of the Riemann surface, the DOS develops a macroscopically degenerate bound state. We present the phase diagram in Fig. 3.

We note that $O(\omega_D)$ term in $C(\omega)$ also contains the combination $\omega_D\ddot{\phi}_0$. As long as ω_D is below the threshold and $\phi_0(\omega)$ approaches $\pi/2$ quadratically, this term only shifts ω_0 by a small amount.

We now include into $C(\omega)$ series of terms with higher powers of $\dot{\phi}_0 \tan\phi_0$. We present computational details in Appendix C and here quote the result: for γ very near 2, the equation on $\phi_0(\omega)$ near ω_0 becomes

$$\dot{\phi}_0\left(1 - \frac{Y}{2(1+Y)} + \frac{\gamma-2}{2}\ln X\right) = \frac{2}{\pi\bar{g}^\gamma}\omega^{\gamma-1}, \tag{54}$$

where $X = \omega_0\dot{\phi}_0\tan\phi_0$ is the same as before, and $Y = \omega_D\dot{\phi}_0\tan\phi_0$. The analysis of Eq. (54) shows that there is again a single line of a topological transition at critical

$$\omega_D^c = \omega_0 e^{-\frac{2}{\gamma-2}}. \tag{55}$$

We see that ω_D^c is finite, although exponentially small for γ slightly above 2.

A finite ω_D also introduces series of terms with higher-order derivatives in $C(\omega)$. The series hold in $\omega_D^{m-1}\phi_0^{(m)}$ ($m \geqslant 2$). We compute these series in Appendix C and argue that they only weakly affect ω_D^c.

VII. PHASE DIAGRAM OF THE γ MODEL

The key result of our analysis is the realization that superconducting state at $\gamma > 2$ is topologically different from the one at $\gamma < 2$. We label these two superconducting states as SC II and SC I, respectively. In both cases, the gap function is analytic in the upper half-plane of frequency, but the gap functions $\Delta_0(z)$ at $\gamma < 2$ and $\gamma > 2$ live on different sheets of the Riemann surface, and at $T = 0$ the DOS in SC II has an edge singularity (a "nonintegrable" singularity at the lower edge of the continuum). The singularity holds up to a finite bosonic mass $\omega_D = \omega_c^*$.

At $T = 0$, we expect a single transition line in the (ω_D, γ) plane between SC I, which holds for all $\omega_D \geqslant 0$ at $\gamma < 2$ and for $\omega_D > \omega_c^*$ at $\gamma > 2$, and SC II, while exists at $\gamma > 2$ in the interval $0 \leqslant \omega_D \leqslant \omega_c^*$. We show the corresponding phase diagram in Fig. 3.

We next consider the phase diagram in the (T, γ) plane at $\omega_D = 0$. Here, we argue, the phases SC I and SC II are separated by a nonsuperconducting, pseudogap phase.

Indeed, in paper V, we demonstrated that for $\gamma = 2$, massless "longitudinal" fluctuations, associated with the continuum spectrum of condensation energies, destroy

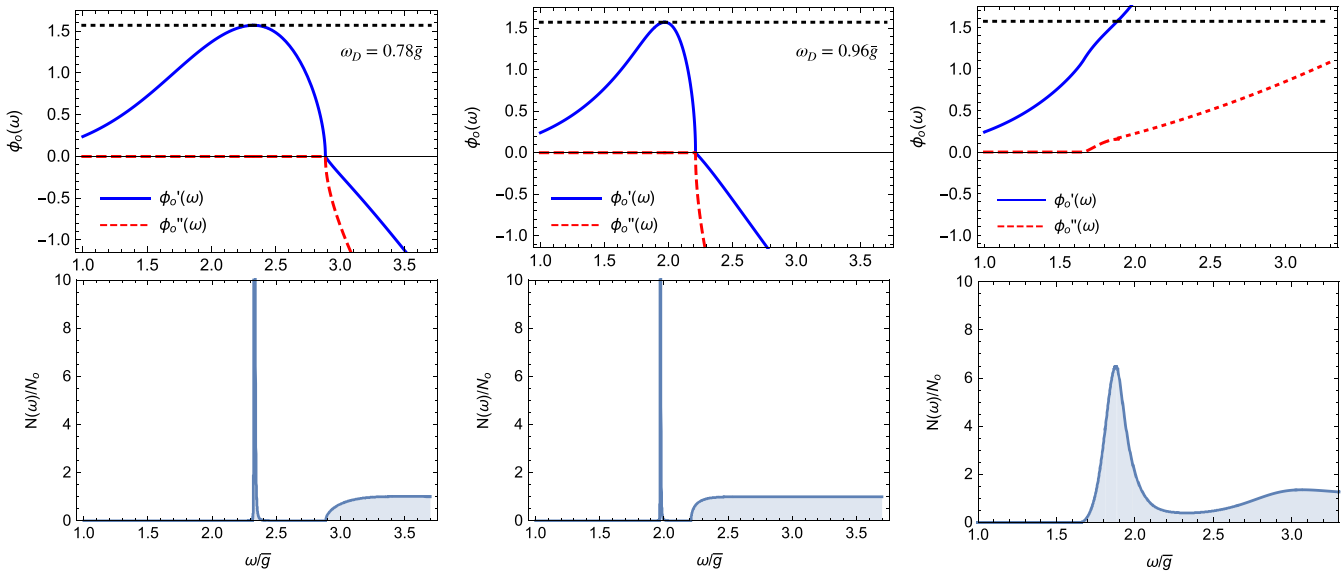

FIG. 25. Numerical results for $\phi_0(\omega)$ and the DOS $N(\omega)$ for a toy model at a finite ω_D. We set $\gamma = 2.7$. As long as ω_D is smaller than the threshold value, the "infinite" peak in $N(\omega)$ survives. Once ω_D exceeds the threshold, the peak moves into the continuum. To get the DOS in (c), we solved Eq. (50) near ω_0, where it is valid, obtained $\mathrm{Im}\phi_0(\omega)$, and smoothly extended it to larger ω.

superconducting order at any finite T, although the onset temperature $T_p = T_{p,0}$ for the pairing is of order $\bar{g}$. Below T_p, bound pairs develop but lack global phase coherence. At $\gamma < 2$ and $\gamma > 2$, longitudinal fluctuations are gapped, and it is natural to expect that T_c becomes nonzero. We argued in paper V that this is the case for SC I, and that T_c increases gradually with $2 - \gamma$. It is natural to assume that SC II also has long-range superconducting order at $T < T_c$, which increases gradually with $\gamma - 2$.

To verify this, we compute the superconducting stiffness ρ_s [the prefactor in $F = \rho_s \int dr \nabla^2 \eta_0(r)$, where $\eta_0(r)$ is the phase of the order parameter $\Delta_0(r) = \Delta_0 e^{i\eta_0(r)}$]. We show the results for different γ and ω_D in Fig. 26. In the calculations, we only included the $n = 0$ solution, i.e., we neglected fluctuation corrections from the solutions with other n.

At small ω_D, the stiffness, expressed in units of E_F, rapidly decreases with increasing γ. Taken at a face value, this would imply that the strength of phase fluctuations rapidly increases with γ. One has to be careful here, however, because our analysis is valid as long as corrections to Eliashberg theory are small. These corrections come from the renormalizations of side vertices in the diagrams for fermionic self-energy and the pairing vertex and hold in powers of the Eliashberg parameter λ_E, which then needs to be at most $O(1)$. For $\gamma = 2$, $\lambda_E = a_2 \bar{g}^2/(E_F \omega_D)$, where $a_2 = O(1)$ (see, e.g., paper V and Ref. [15]). To keep λ_E small at small $\omega_D/\bar{g}$, one need to simultaneously increase E_F. The stiffness ρ_s, expressed in units of the onset temperature for the pairing, T_p, and λ_E, scales as $\rho_s \sim T_p/\lambda_E$. Then, as long as $\lambda_E \leqslant 1$, the ratio ρ_s/T_p does not become small at small ω_D, which implies that phase fluctuations from the $n = 0$ solution alone cannot substantially reduce the actual T_c compared to T_p.

For $\gamma \neq 2$, the Eliashberg parameter is, up to a prefactor, $\lambda_E = a_\gamma \bar{g}^\gamma/(E_F \omega_D^{\gamma-1})$. In panels (b) and (c) of Fig. 26, we plot ρ_s in units of T_p/λ_E, with T_p taken from [16]. We see that this ratio remains finite at $\omega_D \to 0$ for all $\gamma > 1$ and actually increases with γ. This implies that within Eliashberg theory, phase fluctuations from the $n = 0$ solution alone, do not destroy superconducting order even at $\omega_D \to 0$.

A more subtle question is whether for $\gamma > 2$, the order below T_c is SC II, or the SC I/SC II boundary may lay below T_c line. We assume without proof that the phase below T_c at $\gamma > 2$ is SC II. This yields the "symmetric" phase diagram, shown in Fig. 2, with two distinct ordered phases SC I and SC II, and the pseudogap phase in between.

For completeness, in Fig. 27, we show the phase diagram near $\gamma = 2$ with additional set of lines, indicating a cascade of topological transitions at a set of discrete γ, when dynamical vortices cross, one by one, into the upper half-plane of frequency as γ increases towards 2 from either side. The phase winding of $\Delta_0(\omega)$ along the real axis increases by 2π each time a new dynamical vortex moves into the upper half-plane.

VIII. CONCLUSIONS

In this paper, the sixth in the series, we analyzed the interplay between non-Fermi liquid and pairing in the effective low-energy model of fermions with singular dynamical interaction $V(\Omega_m) = \bar{g}^\gamma/|\Omega_m|^\gamma$ (the γ model). The model describes the low-energy physics of various quantum-critical metallic systems at the verge of an instability towards density or spin order as well as pairing of fermions at the half-filled Landau level, color superconductivity, and pairing in SYK-type models (see paper I for the list of microscopic models). In previous publications, paper I–V, we analyzed the physics of the model with $\gamma \leqslant 2$. The key outcome of those studies was that a peculiar quantum-critical behavior develops within the set of these critical models as the exponent γ approaches $\gamma = 2$. Specifically, for any $\gamma < 2$, there is an infinite number of discrete minima of the condensation energy $E_{c,n}$. As γ

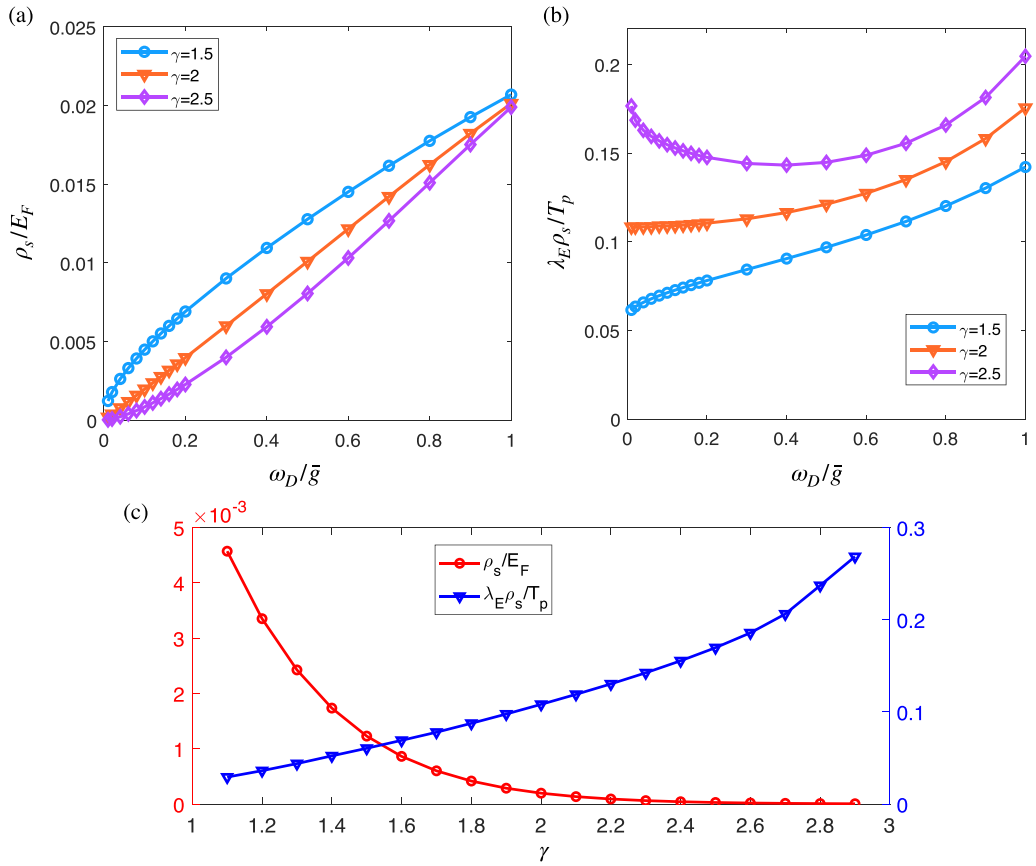

FIG. 26. Numerical results for the superfluid stiffness ρ_s for different γ and ω_D. (a) ρ_s in units of Fermi energy E_F, as a function of ω_D for different γ. For $\gamma > 1$, the stiffness vanishes as $\omega_D^{\gamma-1}$. We verified this dependence analytically. (b) The stiffness in units of T_p/λ_E, where T_p is the onset temperature of the pairing and $\lambda_E = \bar{g}^\gamma/(E_F\omega_D^{\gamma-1})$ is Eliashberg parameter, which measures the strength of corrections to side vertices in the diagrams for the self-energy and the pairing vertex (in commonly accepted language, λ_E measures the strength of vertex corrections to Eliashberg theory). The parameter λ_E has to be smaller than (roughly) one. We see that $\rho_s\lambda_E/T_p$ tends to a finite value at $\omega_D = 0$. This result implies that vertex corrections from only $n = 0$ state do not destroy superconducting order up to $T \leqslant T_p$. (c) Comparable analysis of ρ_s/E_F and $\rho_s\lambda_E/T_p$ at $\omega_D \to 0$.

approaches 2 from below, the set gets more dense, and becomes a continuous one at $\gamma = 2$. Simultaneously, the number of dynamical vortices in the upper half-plane of frequency tends to infinity, and poles approach the boundary of the upper half-plane.

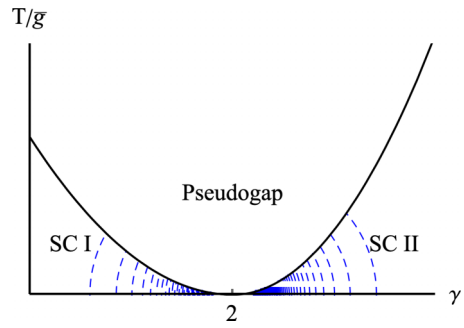

FIG. 27. A cascade of topological transitions, indicated by the set of blue dashed lines around $\gamma = 2$. Upon crossing each line, a dynamical vortex moves into the upper half-plane of frequency, and the total phase variation of $\Delta_0(\omega) = |\Delta_0(\omega)|e^{i\eta(\omega)}$ between $\omega = -\infty$ and $+\infty$ jumps by 2π.

In this paper, we considered the γ model with exponents $2 < \gamma < 3$ and address the issue what happens on the other side of the quantum transition. We argued that the system moves away from criticality, e.g., the spectrum of the condensation energy again becomes discrete, with one particular minimum, corresponding to the gap function $\Delta_0(\omega)$, the number of dynamical vortices in the upper half-plane becomes finite and decreases with increasing γ, and the poles move back into the lower half-plane. However, for this to hold, the gap function has to move to a different sheet of the Riemann surface from the one where it is located at $\gamma < 2$. This makes superconducting states at $\gamma < 2$ and $\gamma > 2$ (phases SC I and SC II, respectively) topologically different and also makes $\gamma = 2$ a topological quantum-critical point.

We found that there is at least one qualitative difference in the behavior of observables in SC I and SC II. Namely, at $\gamma > 2$, the DOS has a nonintegrable singularity at the lower edge of the gapped continuum. In physical terms, this implies that the spectrum of excited states contains a level (a bound

state) with macroscopic degeneracy. We argued that the SC II state exists in a finite range of a mass of a pairing boson, ω_D. We presented the phase diagrams in variables (ω_D, γ) at $T = 0$ (Fig. 3) and in variables (T, γ) at $\omega_D = 0$ (Fig. 2). The last phase diagram contains superconducting phases SC I and SC II and an intermediate state with preformed pairs but no long-range superconducting order.

From physics perspective, the peak in the DOS can be understood using the same reasoning as in Ref. [6], as a bound state between an excitation and an off-diagonal pairing field that this excitation can be modified via the self-energy. Indeed, we find that the self-energy $\Sigma(\omega)$ becomes singular at the lower end of the continuum, where $\Delta(\omega) = \omega$, i.e., at this frequency the effective potential, acting on a fermion in a superconductor, is infinite. A fermion in an infinite potential undergoes a self-trapping that generally leads to bound states. This argument however, does not immediately explains why the bound state is macroscopically degenerate.

The emergence of the nonintegrable singularity may be related to the fact that for $\gamma > 2$, the gap equation on the real axis contains a formally divergent contribution, which needs to be regularized. The divergence comes from the interaction $V(\Omega)$ in the limit of zero frequency transfer $\Omega \to 0$. The interaction $V(\Omega \to 0)$ scatters with vanishingly small frequency transfer and in this respect acts on electrons in the same way as impurities. The contribution from $V(0)$ that cancels out without regularization, is analogous to the contribution from nonmagnetic impurities, while the one, which cancels out only after regularization, is analogous to the contribution from magnetic impurities. In this respect, there may be a similarity between our bound state and Yu-Shiba-Rusinov in-gap bound state in the DOS of a superconductor in the presence of magnetic impurities [17–19].

Finally, the very fact that the leading order in the expansion in $X = \omega\dot{\phi}_0 \tan\phi_0$ captures the divergence in the DOS, but does not capture the power-law singularity at the edge of the continuum, is similar to the situation in the x-ray Fermi edge and Kondo problems (see, e.g., Refs. [20–24] and references therein). From this perspective, one might think that effects similar to the orthogonality catastrophe [25] are also at play in the γ model despite that this model is for a clean system.

ACKNOWLEDGMENTS

We thank I. Aleiner, B. Altshuler, E. Berg, D. Chowdhury, L. Classen, R. Combescot, K. Efetov, R. Fernandes, A. Finkelstein, E. Fradkin, A. Georges, S. Hartnol, S. Karchu, S. Kivelson, I. Klebanov, A. Klein, R. Laughlin, S.-S. Lee, L. Levitov, G. Lonzarich, D. Maslov, F. Marsiglio, I. Mazin, M. Metlitski, W. Metzner, A. Millis, D. Mozyrsky, C. Pepan, V. Pokrovsky, N. Prokofiev, S. Raghu, S. Sachdev, T. Senthil, D. Scalapino, Y. Schattner, J. Schmalian, D. Son, G. Tarnopolsky, A.-M. Tremblay, A. Tsvelik, G. Torroba, Y. Wang E. Yuzbashyan, and J. Zaanen for useful discussions of this and previous works (Papers I-V). The work by Y.-M.W., S.-S.Z, and A.V.C. was supported by the NSF DMR-1834856. Y.-M.W, S.-S.Z., and A.V.C. also acknowledge the hospitality of KITP at UCSB, where part of the work has been conducted. The research at KITP is supported by the National Science Foundation under Grant No. NSF PHY-1748958.

APPENDIX A: KK TRANSFORMATION FOR THE INTERACTION

In this Appendix, we discuss the subtlety with expressing the gap equation on the real axis, Eq. (3), in terms of $C(\omega)$, given by Eq. (19). Taken at a face value, the integral in the r.h.s. of (19) contains the piece

$$-i\bar{g}^{\gamma} \sin\frac{\pi\gamma}{2} \frac{\frac{dD(\omega)}{d\omega}}{\sqrt{1-D^2(\omega)}} \int_{0+}^{\omega} d\Omega \frac{1}{\Omega^{\gamma-1}}. \tag{A1}$$

For $\gamma > 2$, the integral formally diverges and has to be properly regularized.

We went back to the computational steps, involved in the derivation of the gap equation on the real axis, and traced the divergence in the integral for $C(\omega)$ to the divergence in the KK relation for the interaction on the real axis. Specifically, on the real axis,

$$V(\Omega) = \left(\frac{\bar{g}}{|\Omega|}\right)^{\gamma} \left(\cos\frac{\pi\gamma}{2} + i \sin\frac{\pi\gamma}{2} \mathrm{sgn}\Omega\right). \tag{A2}$$

The derivation of $C(\Omega)$ uses the KK relation expressing $V'(\Omega)$ in terms of $V''(\Omega)$:

$$V'(\omega) = \frac{1}{\pi} P \int_{-\infty}^{\infty} \frac{V''(x)}{x-\Omega} = \frac{2}{\pi} P \int_0^{\infty} \frac{V''(x)x}{x^2-\Omega^2}, \tag{A3}$$

where P stands for principle value. Rescaling x by Ω we find that for $V(\Omega)$ from (A2), this relation is satisfied if

$$\frac{2}{\pi} \int_0^{\infty} \frac{dy}{y^{\gamma-1}} \frac{1}{y^2-1} = \cot\frac{\pi\gamma}{2}. \tag{A4}$$

For $\gamma < 2$, this relation holds, as one can easily verify, but for $\gamma > 2$, the integral in the l.h.s. of (A4) diverges.

We argue that to avoid the divergence and satisfy the KK relation for all γ, one has to modify the integration contour to the one shown in Fig. 4, which bypasses $y = 0$ by moving slightly into the upper half-plane of frequency. Indeed, extending $V(\omega)$ into the upper half-plane and integrating in (A3) over the contour in Fig. 4, we find that the integral in the l.h.s. of Eq. (A4) gets modified to

$$\frac{2}{\pi}\left[\int_{\epsilon/\omega}^{\infty} \frac{dy}{y^{\gamma-1}} \frac{1}{y^2-1} + \left(\frac{\omega}{\epsilon}\right)^{\gamma-2} \frac{1}{\gamma-2}\right] \tag{A5}$$

for $2 < \gamma < 4$. The remaining integral is

$$\int_{\epsilon/\omega}^{\infty} \frac{dy}{y^{\gamma-1}} \frac{1}{y^2-1} = -\int_{\epsilon/\omega}^{\infty} \frac{dy}{y^{\gamma-1}} + \int_0^{\infty} \frac{dy y^{(}3-\gamma)}{y^2-1}$$
$$= -\left(\frac{\omega}{\epsilon}\right)^{\gamma-2} \frac{1}{\gamma-2} - \tan\frac{(\gamma-1)\pi}{2}. \tag{A6}$$

Substituting into (A5), we find that the divergent term cancels out, and the KK relation is satisfied. For $\gamma > 4$, the subleading term in (A6) also diverges, and the integral over a half-circle near $z = 0$ has to be computed by including $(\epsilon/\omega)^2$ terms (and higher powers for even larger $\gamma > 6$). We verified that the subleading divergent terms also cancel out, i.e., integrating over

the modified contour one does satisfy the KK relation (A3) for all γ. One can also check that the other KK relation

$$V''(\omega) = -\frac{1}{\pi} P \int_{-\infty}^{\infty} \frac{V'(x)}{x-\Omega} = -\frac{2\Omega}{\pi} P \int_0^{\infty} \frac{V'(x)}{x^2-\Omega^2} \quad \text{(A7)}$$

is also satisfied for all γ, despite that the integral in the r.h.s. of (A7) formally diverges for $\gamma > 1$. The Cauchy relation between $V(\Omega_m)$ and $V''(\Omega)$: $V(\Omega_m) = (1/\pi)\int_0^{\infty} dx V''(x) x/(x^2+\Omega_m^2)$ is also satisfied for the integration contour as in Fig. 4.

In practical terms, bending of the integration contour to by-pass the $z = 0$ point is equivalent to just canceling out the divergent terms in the KK transformation. For $C(\omega)$, this implies that $\int_{0^+}^{\omega} d\Omega/\Omega^{\gamma-1}$ has to be evaluated as

$$\int_{\epsilon}^{\omega} \frac{d\Omega}{\Omega^{\gamma-1}} - \frac{1}{\gamma-2}\frac{1}{\epsilon^{\gamma-2}} = -\frac{1}{\gamma-2}\frac{1}{\omega^{\gamma-2}}. \quad \text{(A8)}$$

Using this procedure, one obtains that the prefactor for the $\dot{\phi}_0$ term in the gap equation evolves smoothly through $\gamma = 2$.

APPENDIX B: THE GAP FUNCTION ALONG THE REAL AXIS

When the critical boson becomes massive, the Eliashberg equantion along the Matsubara axis takes the following form:

$$\Delta(\omega_m) = \bar{g}^{\gamma}\pi T \sum_{\omega_m'} \frac{\Delta(\omega_m') - \Delta(\omega_m)\frac{\omega_m'}{\omega_m}}{\sqrt{(\omega_m')^2 + \Delta^2(\omega_m')}} \times \frac{1}{\left[(\omega_m'-\omega_m)^2 + \omega_D^2\right]^{\gamma/2}}, \quad \text{(B1)}$$

where $\omega_D > 0$ is the mass of the intermediate boson. In this section, we make the analytic continuation of the above equation to the real axis.

To that end, we use the spectral representation of the interaction $\chi(\omega_m) = (1/\pi)\int d\omega \chi''(\omega)/(\omega - i\omega_m)$, where $\chi''(\omega)$ is the imaginary part of the interaction along the real axis

$$\chi(\omega) = \frac{\bar{g}^{\gamma}}{(\omega_D - \omega - i\delta)^{\gamma/2}(\omega_D + \omega + i\delta)^{\gamma/2}}, \quad \text{(B2)}$$

where δ is an infinitesimal positive number. Noting that $\mathrm{Arg}[(\omega_D - \omega - i\delta)(\omega_D + \omega + i\delta)] = -\pi \mathrm{sign}\omega\Theta(|\omega| - \omega_D)$, we have

$$\chi'(\omega) = \frac{\bar{g}^{\gamma}}{\left(|\omega|^2 - \omega_D^2\right)^{\gamma/2}}\Theta(\omega_D - |\omega|) + \frac{\bar{g}^{\gamma}}{\left(|\omega|^2 - \omega_D^2\right)^{\gamma/2}}\cos\left(\frac{\pi\gamma}{2}\right)\Theta(|\omega| - \omega_D), \quad \text{(B3)}$$

$$\chi''(\omega) = \frac{\bar{g}^{\gamma}}{\left(|\omega|^2 - \omega_D^2\right)^{\gamma/2}}\sin\left(\frac{\pi\gamma}{2}\right)\mathrm{sign}\omega\Theta(|\omega| - \omega_D). \quad \text{(B4)}$$

With this representation, the gap equation can be rewritten as

$$\Delta(\omega_m) = \int_{-\infty}^{\infty} d\omega \chi''(\omega)\left(T\sum_{\omega_m'} \frac{\Delta(\omega_m') - \Delta(\omega_m)\frac{\omega_m'}{\omega_m}}{\sqrt{(\omega_m')^2 + \Delta^2(\omega_m')}} \frac{1}{\omega - i(\omega_m - \omega_m')}\right). \quad \text{(B5)}$$

Now we make the analytic continuation $i\omega_m \to z$, while keeping the terms within the bracket analytic on the upper complex plane:

$$\begin{aligned} & T\sum_{\omega_m'} \frac{\Delta(\omega_m') - \Delta(\omega_m)\frac{\omega_m'}{\omega_m}}{\sqrt{(\omega_m')^2 + \Delta^2(\omega_m')}} \frac{1}{\omega - i(\omega_m - \omega_m')} \\ & \to T\sum_{\omega_m'} \frac{\Delta(\omega_m')}{\sqrt{(\omega_m')^2 + \Delta^2(\omega_m')}} \frac{1}{\omega - z + i\omega_m'} - \frac{\Delta(\omega_m)}{\omega_m} T\sum_{\omega_m'} \frac{\omega_m'}{\sqrt{(\omega_m')^2 + \Delta^2(\omega_m')}} \frac{1}{\omega - z + i\omega_m'} \\ & - \frac{1}{2}\frac{\Delta(z-\omega)}{\sqrt{-(z-\omega)^2 + \Delta^2(z-\omega)}}\left(\tanh\frac{\omega - z}{2T} - \coth\frac{\omega}{2T}\right) + \frac{1}{2}\frac{\Delta(z)}{z}\frac{z-\omega}{\sqrt{-(z-\omega)^2 + \Delta^2(z-\omega)}}\left(\tanh\frac{\omega - z}{2T} - \coth\frac{\omega}{2T}\right). \end{aligned} \quad \text{(B6)}$$

The additional terms except that from the replacement $i\omega_m \to z$ ensure that the extended function of z gets rid of the pole at $z = \omega + i\omega_m'$ ($|\omega| > \omega_D$). The gap equation on the upper complex plane takes the form

$$\begin{aligned} zD(z) = {} & \pi T \sum_{\omega_m'} \frac{\Delta(\omega_m')}{\sqrt{(\omega_m')^2 + \Delta^2(\omega_m')}} \chi(\omega_m' + iz) \\ & - iD(z)\pi T \sum_{\omega_m'} \frac{\omega_m'}{\sqrt{(\omega_m')^2 + \Delta^2(\omega_m')}} \chi(\omega_m' + iz) \\ & - \frac{1}{2}\int_{-\infty}^{\infty} d\omega \chi''(\omega) \frac{\Delta(z-\omega) - (z-\omega)D(z)}{\sqrt{-(z-\omega)^2 + \Delta^2(z-\omega)}} \\ & \times \left(\tanh\frac{\omega - z}{2T} - \coth\frac{\omega}{2T}\right), \end{aligned} \quad \text{(B7)}$$

where $D(z) = \Delta(z)/z$ and $V(-iz) = (\bar{g}^2/(\omega_D^2 - z^2))^{\gamma/2}$. In a compact form, we have

$$zD(z)B(z) = A(z) + C(z),$$

where

$$A(z) = \pi T \sum_{\omega'_m>0} \frac{D(\omega'_m)}{\sqrt{1+D^2(\omega'_m)}}(\chi(\omega'_m+iz)+\chi(\omega'_m-iz)), \tag{B8}$$

$$B(z) = 1 + i\frac{\pi T}{z}\sum_{\omega'_m>0}\frac{1}{\sqrt{1+D^2(\omega'_m)}}(\chi(\omega'_m+iz) - \chi(\omega'_m-iz)), \tag{B9}$$

$$C(z) = -\frac{1}{2}\int_{-\infty}^{\infty} d\omega\chi''(\omega)\frac{\Delta(z-\omega)-(z-\omega)D(z)}{\sqrt{-(z-\omega)^2+\Delta^2(z-\omega)}} \times\left(\tanh\frac{\omega-z}{2T}-\coth\frac{\omega}{2T}\right). \tag{B10}$$

Below we consider the real axis where we replace z by $\omega+i\delta$. At zero temperature, using the spectral representation of the interaction $\chi(\omega)$, the above functions reduce to

$$A(\omega) = \frac{1}{2}\int_0^\infty d\omega_m \frac{D(\omega_m)}{\sqrt{1+D^2(\omega_m)}}(\chi(\omega_m+i\omega) + \chi(\omega_m-i\omega)) \tag{B11}$$

$$B(\omega) = 1 + \frac{i}{2z}\int_0^\infty d\omega_m \frac{1}{\sqrt{1+D^2(\omega_m)}}(\chi(\omega_m+i\omega) - \chi(\omega_m-i\omega)) \tag{B12}$$

$$C(\omega) = \frac{i}{2}\int_0^{|\omega|} d\Omega\chi''(\Omega)\frac{D(\omega-\Omega)-D(\omega)}{\sqrt{1-D^2(\omega-\Omega)}}. \tag{B13}$$

Once we obtained $D(\omega_m)$ by solving the Eliashberg equation along the Matsubara axis, $A(\omega)$ and $B(\omega)$ are known functions.

APPENDIX C: EXPANSION OF $C(\omega)$

We evaluate $C(\omega)$ in (19) by Taylor-expanding the integrand in powers of internal Ω, integrating each term in the expansion, and summing up the series. This procedure is inspired by the fact that only one term in the series survives at $\gamma = 2$. However, away from this γ, an infinite number of terms appear with the same prefactor $(\gamma-2)$, and one has to sum up infinite series.

1. At a QCP

We first consider the case at a QCP and perform the integral over Ω at each order of the expansion:

$$\int_0^\omega \frac{d\Omega}{\Omega^\gamma}\Omega^n = \frac{\omega^{n+1-\gamma}}{n+1-\gamma}, n = 1, 2, \ldots \tag{C1}$$

The infrared divergence for $n = 1$ is avoided using the trick discussed in Appendix A. The expansion of $C(\omega)$ is then given by a differential form

$$\begin{aligned} C(\omega) = \frac{\bar{g}^\gamma}{\omega^{\gamma-2}}\frac{\sin\frac{\pi\gamma}{2}}{2-\gamma}D(\omega)\Big\{&\dot\phi + \frac{\gamma-2}{2(3-\gamma)}\omega[\tan\phi\dot\phi^2+\ddot\phi] - \frac{\gamma-2}{6(4-\gamma)}\omega^2[(2+3\tan^2\phi)\dot\phi^3 + 3\tan\phi\dot\phi\ddot\phi + \dddot\phi] \\ &+ \frac{\gamma-2}{24(5-\gamma)}\omega^3[(11\tan\phi+12\tan^3\phi)\dot\phi^4 + (12+18\tan^2\phi)\dot\phi^2\ddot\phi + 3\tan\phi\ddot\phi^2 + 4\tan\phi(\dot\phi)(\dddot\phi) + \phi^{(4)}] \\ &- \frac{\gamma-2}{120(6-\gamma)}\omega^4[(16+75\tan^2\phi+60\tan^4\phi)\dot\phi^5 + (110\tan\phi+120\tan^3\phi)\dot\phi^3\ddot\phi \\ &+(20+30\tan^2\phi)\dot\phi^2\dddot\phi + 5(6+9\tan^2\phi)\dot\phi\ddot\phi^2 + 5\tan\phi\dot\phi\phi^{(4)} + 10\tan\phi(\ddot\phi)(\dddot\phi) + \phi^{(5)}] + \ldots\Big\}. \end{aligned} \tag{C2}$$

The order of this expansion is equal to the number of derivatives with respect to ω (denoted as M). The leading order $M = 1$ survives at $\gamma-2$. All the higher order terms are proportional to the small parameter $\gamma-2$. Clearly, the small-Ω expansion is not equivalent to a small-$(\gamma-2)$ expansion.

As we are mainly interested in the gap function around ω_0, where $\phi = \pi/2$ and $\tan\phi = \infty$, we choose the highest power of $\tan\phi$ in the coefficients of each differential term in Eq. (C2). Keeping only the first derivative terms gives rise to

$$C(\omega) = \frac{\bar{g}^\gamma}{\omega^{\gamma-2}}\frac{\sin\frac{\pi\gamma}{2}}{2-\gamma}D(\omega)\dot\phi\left[1+\frac{\gamma-2}{2(3-\gamma)}X - \frac{\gamma-2}{2(4-\gamma)}X^2\frac{\gamma-2}{2(5-\gamma)}X^3+\ldots\right], \tag{C3}$$

namely Eq. (28) in the main text, where $X = \omega\tan\phi\dot\phi$. This leads to the gap equation in Eq. (29), which has been analyzed in Sec. V B.

Now we examine the effect of terms with higher derivatives (e.g., $\ddot\phi$, $\dddot\phi$, etc.). To simplify the discussion, we consider the case $\gamma = 2+0$, for which without higher derivatives we have at ω slightly below ω_0: $\phi = \pi/2 + Q(\omega_0-\omega)/\ln(1-\omega/\omega_0)$ with $Q = 4\omega_0^{\gamma-1}/[\pi(\gamma-2)\bar{g})^\gamma]$ [see Eq. (41)] and check how this behavior is affected by terms with higher derivatives. The contributions of these terms to $C(\omega)$ is

$$-\frac{\bar{g}^\gamma\sin\frac{\pi\gamma}{2}}{\omega^{\gamma-2}}D_0(\omega)\left[\frac{1}{2!}\omega\ddot\phi\left(1-\frac{1}{2}X+\frac{1}{2}X^2-\frac{1}{2}X^3+\ldots\right) - \frac{1}{3!2}\omega^2\dddot\phi\left(1-\frac{2}{3}X+\frac{3}{4}X^2-\frac{4}{5}X^3+\ldots\right) + \frac{1}{4!3}\omega^3\ddddot\phi\left(1-\frac{3}{4}X(1-\frac{6}{5}X+\frac{8}{6}X^2+\ldots)\right) - \ldots\right]. \tag{C4}$$

The prefactor for each term is a particular series in X. Summing up these series and using the fact at $\omega \approx \omega_0$, X is large, we find that each series sums up to $1/2$. The expression in the square brackets in (C4) then becomes

$$\frac{1}{2}\left(\frac{1}{2!}\omega\ddot{\phi} - \frac{1}{3!2}\omega^2\dddot{\phi} + \frac{1}{4!3}\omega^3\ddddot{\phi} - \dots\right) \tag{C5}$$

To understand whether the terms with higher derivatives are important, we substitute into this expressions the values of $\dot{\phi}$, $\dddot{\phi}$, etc, obtained using previous result for $\phi(\omega)$, Eq. (41). From that formula, $\dot{\phi} = Q/\ln X$ and $\omega_0^{n-1}\phi^{(n\geqslant 2)} = -(n-2)!QX^{n-1}/\ln^2 X$. Substituting these expressions, we rewrite Eq. (C5) as

$$-2\frac{Q}{\ln^2 X}\sum_{m=0}^{\infty}\frac{(-1)^m X^{m+1}}{(m+1)^2(m+2)}. \tag{C6}$$

With these contributions, the gap equation gets modified to

$$\dot{\phi}\left[1 + \frac{\gamma-2}{2}[\ln(1+X)+K]\right] = \frac{2\omega^{\gamma-1}}{\pi\bar{g}^{\gamma}}, \tag{C7}$$

where K is given by Eq. (44) in the main text. At large X, $K \approx -(1/2)\ln X$. We see therefore that the terms with higher derivatives do not change the functional form of the gap equation and only add $1/2$ to the prefactor for the $\ln(1+X)$ term.

2. A finite ω_D

Next, we consider the effect of a finite but small mass ($\omega_D > 0$) of the critical boson. We redo the integral over Ω in the presence of a finite ω_D:

$$\int_{\omega_D}^{\omega}\frac{d\Omega}{\left(\Omega^2-\omega_D^2\right)^{\gamma/2}}\Omega^n = \frac{\omega_D^{n+1-\gamma}}{2}B_{1-(\frac{\omega_D}{\omega})^2}\left(1-\frac{\gamma}{2},\frac{\gamma-n-1}{2}\right), \tag{C8}$$

where $B_z(a,b)$ refers to the incomplete Beta function. The divergence at $\Omega = \omega_D$ at $\gamma > 2$ is again avoided using the trick discussed in Appendix A. Near $\gamma = 2$, this integral depends on the ratio between ω_D^{n-1} and $\gamma - 2$, i.e.,

$$\int_{\omega_D}^{\omega}\frac{d\Omega}{\left(\Omega^2-\omega_D^2\right)^{\gamma/2}}\Omega^n = \frac{1}{2-\gamma}\omega_D^{n-1} + \mathcal{O}((2-\gamma)^0). \tag{C9}$$

The function $C(\omega)$, however, is regular because $1/(2-\gamma)$ is canceled out by the small factor $\sin(\pi\gamma/2)$ from the interaction function. Subtracting the contribution at $\omega_D = 0$ and keeping only the leading order in $\gamma - 2$, we obtain the modification to $C(\omega)$ due to a finite mass in the form

$$\begin{aligned}\frac{\bar{g}^{\gamma}}{\omega^{\gamma-2}}\frac{\sin\frac{\pi\gamma}{2}}{2-\gamma}D(\omega)\Bigg[&-\frac{1}{2}\dot{\phi}(Y - Y^2 + Y^3 - Y^4 + \dots)\\ &-\left(\frac{1}{2!}\omega_D\ddot{\phi} - \frac{1}{3!}\omega_D^2\dddot{\phi} + \frac{1}{4!}\omega_D^3\ddddot{\phi} + \dots\right)\\ &\times\left(1 - Y + \frac{3}{2}Y^2 - 2Y^3 + \frac{5}{2}Y^4 + \dots\right)\Bigg],\end{aligned} \tag{C10}$$

where $Y = \omega_D\tan\phi\dot{\phi}$.

Ignoring the terms with second and higher order derivatives, we obtain the result presented in Eq. (54). From that expression, we obtained in the main text the critical ω_D^c, Eq. (55). This critical ω_D^c is determined by $Y = O(1)$ and $X \gg 1$ (relevant $X \approx Y\omega_0/\omega_D \gg Y$).

To estimate the role of the terms with higher derivatives in (C10), we evaluate them at the same $Y = O(1)$ and $X \gg 1$. The series $1 - Y + 3Y^2/3 - 2Y^3 + 5Y^4/2$ sum up to $O(1)$ at $Y = O(1)$. For the series $\omega_D\ddot{\phi}/2! - \omega_D^2\dddot{\phi}/3! + \omega_D^3\ddddot{\phi}/4! + \dots$ we borrow the result from the previous Section and obtain

$$\begin{aligned}&\frac{1}{2!}\omega_D\ddot{\phi} - \frac{1}{3!}\omega_D^2\dddot{\phi} + \frac{1}{4!}\omega_D^3\ddddot{\phi} + \dots\\ &= -\frac{Q}{\ln^2 X}Y\sum_{m=0}^{\infty}\frac{(-1)^m}{(m+1)(m+2)}Y^m\\ &= -\frac{Q}{\ln^2 X}\left(\frac{1+Y}{Y}\ln(1+Y) - \frac{1}{Y}\right)\\ &= -\frac{\dot{\phi}}{\ln X}\left(\frac{1+Y}{Y}\ln(1+Y) - \frac{1}{Y}\right)\end{aligned} \tag{C11}$$

For $Y = O(1)$, this is of order $-\frac{\dot{\phi}}{\ln X}$. For the same $Y = O(1)$, the first term in (C10) is of order $\dot{\phi}$, i.e., is larger by $\ln X$. This implies that the terms with higher derivatives can be safely neglected.

APPENDIX D: THE $n = \infty$ SOLUTION ON THE UPPER COMPLEX PLANE

The $n = \infty$ solution along the Matsubara axis is given analytically by the same expression as for $\gamma \leqslant 2$, and we refer to Refs. [1,4,5] for details. Its analytic continuation towards the upper complex plane of frequency is obtained by a rotation of frequency axis, $i\omega_m \to z = \omega' + i\omega'' = |z|e^{i\psi}$, which gives rise to

$$\Delta_{\infty}(z) = \int_{-\infty}^{\infty}dk\frac{e^{-\theta k}e^{-iI_k - ik\ln y_z}}{\sqrt{\cosh(\pi(k-\beta))\cosh(\pi(k+\beta))}}, \tag{D1}$$

where $y_z = (|z|/\bar{g})^{\gamma}$, $\theta = (\pi/2 - \psi)\gamma$, and

$$b_k = \frac{e^{-i(I_k + k\ln(\gamma-1))}}{[\cosh(\pi(k-\beta))\cosh(\pi(k+\beta))]^{1/2}}. \tag{D2}$$

Here

$$I_k = \frac{1}{2}\int_{-\infty}^{\infty}dk'\ln|\epsilon_{k'} - 1|\tanh\pi(k'-k), \tag{D3}$$

$$\begin{aligned}\epsilon_{k'} = &\frac{1-\gamma}{2}\frac{\Gamma\left(\frac{\gamma}{2}(1+2ik')\right)\Gamma\left(\frac{\gamma}{2}(1-2ik')\right)}{\Gamma(\gamma)}\\ &\times\left(1 + \frac{\cosh\pi\gamma k'}{\cos\pi\gamma/2}\right),\end{aligned} \tag{D4}$$

and $\beta > 0$ is the solution of $\epsilon_{\beta} = 1$. This extension is limited to the region $-\pi/\gamma < \psi - \pi/2 < \pi/\gamma$ where the integral giving rise to $\Delta_{\infty}(z)$ is convergent. The critical axis $\psi = \pi/2 \pm \pi/\gamma$ is on the lower complex plane when $\gamma < 2$, and rotates to the upper plane when $\gamma > 2$. Along the critical axis, the behavior of $\Delta_{\infty}(z)$ is very similar to that along the real axis at $\gamma = 2$, where the phase $\eta_{\infty}(z) = \mathrm{Arg}(D_{\infty}(z))$ winds up to infinity as $|z| \to \infty$, while the amplitude follows a power-law increase $\sim|z|^{\gamma/2/(\gamma-1)}$. The phase winding is attributed to the existence of an array of infinite vortices that line up along the

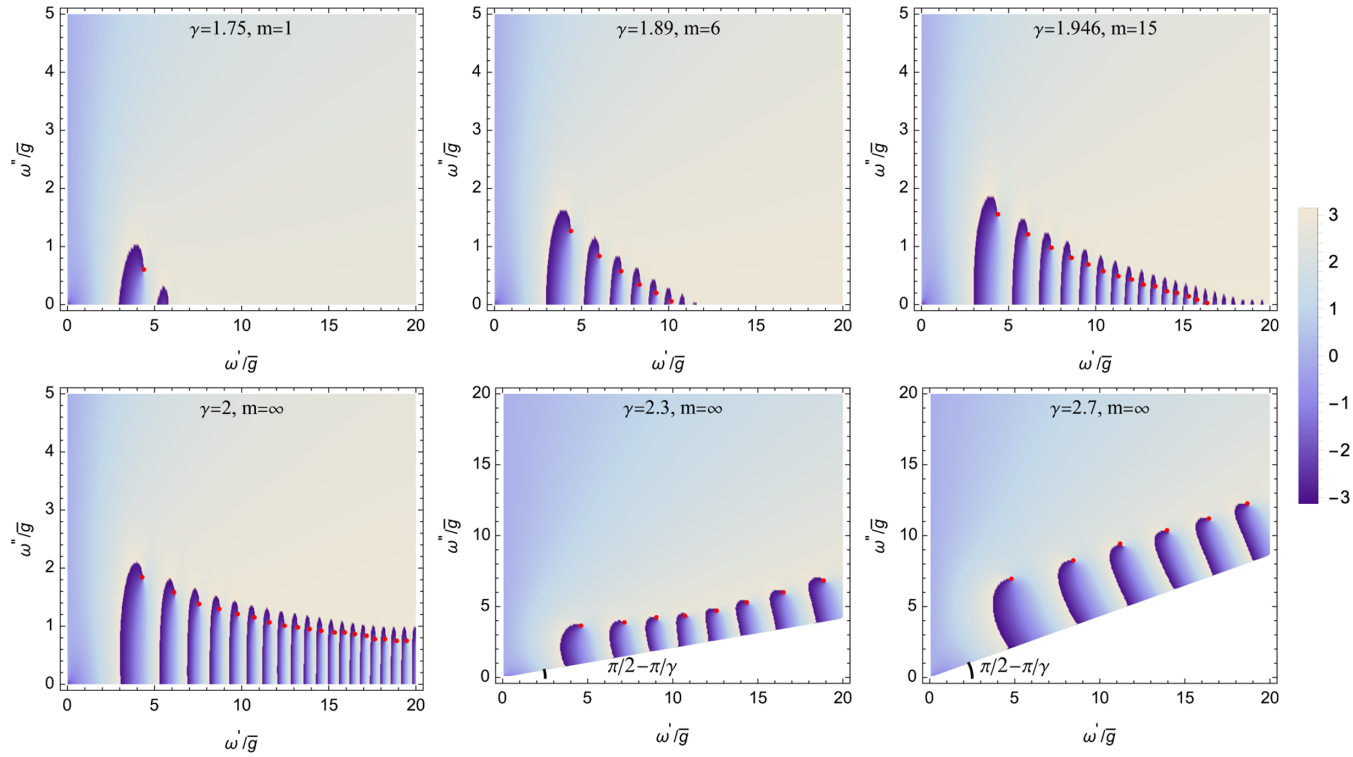

FIG. 28. Vortices of the gap function $\Delta_\infty(z)$ in the upper half-plane of frequency for representative γ between 1 and 3 ($z = \omega' + i\omega''$). These vortices form an array, pointing along the axis $\arg(z) = \pi/2 - \pi/\gamma$. This axis rotates from the lower half-plane at $\gamma < 2$ towards the upper half-plane at $\gamma > 2$. It coincides with the real axis at the critical point $\gamma = 2$.

critical axis as $|z| \to \infty$. Consequently, there is only a finite number of vortices in the upper half-plane when $\gamma < 2$, but the number becomes infinite for $\gamma \geqslant 2$. We illustrate this in Fig. 28.

APPENDIX E: A DISCRETE SET OF SOLUTIONS OF THE NONLINEAR GAP EQUATION

Here we present the details of the analysis of a discrete set of solutions $\Delta_n(\omega_m)$. We depart from the solution of the linearized gap equation and expand the solution of the full nonlinear gap equation in powers of Δ as

$$\Delta(\omega_m) = \sum_{j=0}^{\infty} \epsilon^{2j+1} \Delta^{(2j+1)}(\omega_m), \tag{E1}$$

where $\Delta^{(1)}(\omega_m) = \Delta_\infty(\omega_m)$. We then solve iteratively for $\Delta^{(2j+1)}$ in terms of $\Delta^{(2j'+1)}$ and $j' < j$.

The gap equation must be satisfied at each order of ϵ, which imposes the following equation:

$$\omega_m D^{(2j+1)}(\omega_m) - \frac{\bar{g}^\gamma}{2} \int_{-\infty}^{\infty} d\omega'_m (D^{(2j+1)}(\omega'_m) - D^{(2j+1)}(\omega_m)) \frac{\mathrm{sign}(\omega'_m)}{|\omega'_m - \omega_m|^\gamma} = K^{(2j+1)}(\omega_m), \tag{E2}$$

with $j = 0, 1, 2, \ldots$ The source term $K^{(2j+1)}(\omega_m)$ is built from the gap function of a lower order $1 \leqslant j' < j$. For example, the first two orders are given by

$$K^{(0)}(\omega_m) = 0, \tag{E3}$$

$$K^{(3)}(\omega_m) = -\frac{\bar{g}^\gamma}{4} \int_{-\infty}^{\infty} d\omega'_m \frac{\mathrm{sgn}(\omega'_m)}{|\omega'_m - \omega_m|^\gamma} \times (D^{(1)}(\omega'_m) - D^{(1)}(\omega_m)) D^{(1)2}(\omega'_m). \tag{E4}$$

Since $K^{(0)}(\omega_m) = 0$, the leading order is given by the solution of the linearized gap equation

$$D^{(1)}(\omega_m) = D_\infty(\omega_m). \tag{E5}$$

At $\omega \ll \bar{g}$, there is

$$D^{(1)}(\omega_m) \to 2\mathrm{sgn}(\omega_m) \left(\frac{|\omega_m|}{\bar{g}} \right)^\delta \cos f(\omega_m), \tag{E6}$$

where $\delta = (\gamma - 2)/2$ and

$$f(\omega_m) = \beta \ln \frac{|\omega_m|^\gamma}{\bar{g}^\gamma} + \phi. \tag{E7}$$

We note that the term $\omega_m D^{(0)}(\omega_m)$ in the gap equation is irrelevant for the small frequency behavior. This holds true for each subleading order to be discussed.

Provided the leading order $j = 0$ solved, one can compute the source term at the next order, $K^{(3)}(\omega)$, and then search for the induced solution $D^{(3)}(\omega_m)$. For the smallest frequency, $K^{(3)}(\omega)$ is free from the ultra-violet details, and thus fully determined by the asymptotic form of $D^{(1)}(\omega)$ in Eq. (E6). One can continue this process to higher orders, which is summarized as a two-step iterative procedure. (1) Once we found the solution at orders $j' < j$, we first compute the source term

at order j:

$$K^{(j)}(\omega_m) = \bar{g}\left(\frac{|\omega_m|}{\bar{g}}\right)^{(j-\frac{1}{2})(\gamma-2)-1} \times \sum_{r=0}^{j} e^{i(2r+1)f(\omega_m)} I_{2r+1}^{(2j+1)} + c.c., \tag{E8}$$

where $I_{2r+1}^{(2j+1)}$ is determined from the lower-order solutions. For $j = 1$, we use the $j = 0$ solution and obtain

$$I_1^{(3)} = -\tfrac{1}{4} I(3\delta + i\beta\gamma, 2\delta + 2i\beta\gamma) - \tfrac{1}{2} I(3\delta + i\beta\gamma, 2\delta), \tag{E9}$$

$$I_3^{(3)} = -\tfrac{1}{4} I(3\delta + 3i\beta\gamma, 2\delta + 2i\beta\gamma). \tag{E10}$$

Here we have defined the integrals

$$\begin{aligned} I(a,b) &= \int_{-\infty}^{\infty} \frac{dx}{|x-1|^{\gamma}} (|x|^a - \mathrm{sign}(x)|x|^b) \\ &= B(\gamma - 1 - a, 1 + a) + B(\gamma - 1 - b, 1 + b) \\ &\quad + \frac{\pi \csc(\pi\gamma)}{\Gamma(\gamma)} \left(\frac{\Gamma(1+a)}{\Gamma(2-\gamma+a)} - \frac{\Gamma(1+b)}{\Gamma(2-\gamma+b)} \right. \\ &\quad \left. + \frac{\Gamma(\gamma-1-a)}{\Gamma(-a)} - \frac{\Gamma(\gamma-1-b)}{\Gamma(-b)} \right), \end{aligned} \tag{E11}$$

where $B(x, y)$ is the Beta function. The convergence of this integral requires $\gamma < 3$ and $-1 < \mathrm{Re}[a], \mathrm{Re}[b] < \gamma - 1$. On order $j = 1$, it requires $\gamma < 3$; on an arbitrary order $j > 1$, it requires $\gamma < 2 + 2/(2j-1)$.

(2) The source term in Eq. (E8) leads to the induced solution at order j:

$$D^{(j)}(\omega_m) \simeq 2\mathrm{sgn}(\omega_m) \left(\frac{|\omega_m|}{\bar{g}}\right)^{(2j+1)\delta} \times \sum_{r=0}^{j} Q_{2r+1}^{(2j+1)} \cos\left((2r+1)f(\omega_m) + \phi_{2r+1}^{(2j+1)}\right). \tag{E12}$$

where

$$Q_{2r+1}^{(2j+1)} \exp\left[i\phi_{2r+1}^{(2j+1)}\right] = -2I_{2r+1}^{(2j+1)} \Big/ J_{2r+1}^{(2j+1)}, \; r = 0, 1, \ldots, j; \tag{E13}$$

and

$$J_{2r+1}^{(2j+1)} = I((2j+1)\delta + i\beta\gamma(2r+1), 0). \tag{E14}$$

The integrals $J_{2r+1}^{(2j+1)}$ is convergent under the same condition as $I_{2r+1}^{(2j+1)}$.

To apply the above iterative procedure for any given $\gamma > 2$, however, we must stop at a finite order $j \sim 1/(\gamma - 2)$, above which, the gap function cannot be satisfied because the divergence in both integrals $I_{2r+1}^{(2j+1)}$ and $J_{2r+1}^{(2j+1)}$ cannot be canceled out from the equation. The divergence indicates the gap equation at the low-frequency limit depends on the gap function at the higher frequency, which in turns depends on the parameter ϵ. In other words, ϵ enters the gap equation at each order by renormalizing the divergence. To satisfy the gap equation, only a discretized set of ϵ is possible, indicating that the solutions form an infinite and discrete set.

APPENDIX F: BEHAVIOR OF $\Delta_0(\omega_m)$ IN THE EXTENDED γ MODEL AT $M \to 0$

The numerical solution in Fig. 12(b) for $\gamma > 2$ shows that $\Delta_0(\bar{\omega}_m)$, where $\bar{\omega}_m$ is a properly normalized frequency, vanishes at $M = 0$ in a rather peculiar way: the gap function at zero frequency, $\Delta_0(0)$, gradually decreases as M gets smaller and vanishes at $M = 0$, however the full function $\Delta_0(\bar{\omega}_m)$ remains finite at $M = 0+$ and scales as $\bar{\omega}_m$ at small frequencies.

In this section, we analyze the behavior of $\Delta_0(\bar{\omega}_m)$ analytically and argue that at $M = 0+$, there exists a one-parameter continuous set $\Delta_{0,\varepsilon}(\bar{\omega}_m)$, specified by a parameter ε, which runs between $\varepsilon_{\min} = 0+$ and a finite $\varepsilon_{\max}$. All $\Delta_{0,\varepsilon}(\bar{\omega}_m)$ vanish at $\bar{\omega}_m = 0$ and scale linearly with $\bar{\omega}_m$ at small frequencies, but the slope is proportional to ε. As M approaches zero from the positive side, the gap function $\Delta_0(\bar{\omega}_m)$ approaches $\Delta_{0,\varepsilon_{\max}}(\bar{\omega}_m)$, while as M approaches zero from the negative side, the gap function is infinitesimally small and approaches $\Delta_{0,\varepsilon_{\min}}(\bar{\omega}_m)$,

The gap function with $\varepsilon_{\min}$ is the solution of the linearized gap equation. At small frequencies, $\Delta_{0,\varepsilon_{\min}}(\bar{\omega}_m)$ is the sum of two power-laws $(\bar{\omega}_m)^{a_{1,2}}$. At $M \to 0$, a_1 approaches 1 and a_2 approaches $\gamma - 1 > 1$, hence $(\bar{\omega}_m)^{a_1}$ is much larger, hence $\Delta_{0,\varepsilon_{\min}}(\bar{\omega}_m)$ is linear in $\bar{\omega}_m$ at small frequencies. Like we said, the numerical solution of the nonlinear gap equation at $M \to 0$ also shows linear dependence of the gap function on frequency at small $\bar{\omega}_m$. Based on this analogy, we assume that at $M \to 0$, there is a set of gap functions $\Delta_{0,\varepsilon}(\bar{\omega}_m)$, which at small $\bar{\omega}_m$ are all linear in $\bar{\omega}_m$ at $M = 0+$ and at vanishingly small but finite M behave as $\Delta_{0,\varepsilon}(\bar{\omega}_m) = \varepsilon|\bar{\omega}_m|^{1+\delta}\mathrm{sign}(\bar{\omega}_m)$, where δ scales with M.

To determine the two parameters ε and δ, we substitute this trial function into the modified gap equation in Eq. (11). In the infrared limit, the bare $\bar{\omega}_m$ term in the l.h.s. is irrelevant, and ignoring it we rewrite Eq. (11) as

$$\begin{aligned} &\int \frac{d\bar{\omega}'_m}{|\bar{\omega}_m - \bar{\omega}'_m|^{\gamma}} \left(\frac{|D(\bar{\omega}_m)|}{\sqrt{1 + D^2(\bar{\omega}_m)}} - \frac{|D(\bar{\omega}'_m)|}{\sqrt{1 + D^2(\bar{\omega}'_m)}} \right) \\ &= MD(\bar{\omega}_m) \int \frac{d\bar{\omega}'_m}{|\bar{\omega}_m - \bar{\omega}'_m|^{\gamma}} \\ &\quad \times \left(\frac{\mathrm{sign}(\bar{\omega}_m)}{\sqrt{1 + D^2(\bar{\omega}_m)}} - \frac{\mathrm{sign}(\bar{\omega}'_m)}{\sqrt{1 + D^2(\bar{\omega}'_m)}} \right). \end{aligned} \tag{F1}$$

Substituting the trial function into this equation, expanding to order ϵ^3, and evaluating the integrals which turn out to be convergent in the infrared and ultra-violet limits, we obtain at vanishing δ

$$\frac{\delta}{2} I(\gamma)(1 - \varepsilon^2 + \mathcal{O}(\varepsilon^4)) = \frac{M}{\gamma - 1} + \mathcal{O}(M\varepsilon^2), \tag{F2}$$

where

$$\begin{aligned} I(\gamma) &= -\int_0^{\infty} dx \ln x \left(\frac{1}{|1-x|^{\gamma}} + \frac{1}{(1+x)^{\gamma}} \right) \\ &= \frac{1}{\gamma - 1} \left(H(\gamma - 2) - H(1 - \gamma) + \frac{\pi}{\sin \pi\gamma} \right) \end{aligned} \tag{F3}$$

and $H(x)$ is the Harmonic number, analytically continued from $H(n) = \sum_{k=1}^{n} 1/k$. In the two limits, $I(\gamma) \simeq \pi^2(\gamma -$

$2)/2$ near $\gamma = 2$ and $I(\gamma) \simeq 1/(3-\gamma)$ near $\gamma = 3$. We see that $\delta \propto M$, as we anticipated.

Equation (F2) sets one condition on two parameters, δ and ε and therefore allows for a continuous set of solutions. Taking the limit $M \to 0$ and keeping $\delta/M = \alpha > 0$ as a constant, we obtain ε as a function of α:

$$\varepsilon = \sqrt{1 - \frac{2}{(\gamma-1)I(\gamma)}\frac{1}{\alpha}}. \tag{F4}$$

As α varies between $(\gamma-1)I(\gamma)/2$ and ∞, the amplitude parameter ε changes continuously from $\varepsilon_{\min} = 0+$ to $\varepsilon_{\max} = 1$. The gap function with $\varepsilon_{\min}$ is the solution of the linearized gap equation, which is also the only solution one can obtain by approaching $M = 0$ from negative M, while the solution with $\varepsilon_{\max}$ is $\Delta_0(\bar{\omega}_m)$ that we obtained numerically by solving the nonlinear gap equation at $M \to 0$ coming from positive M.

[1] A. Abanov and A. V. Chubukov, Interplay between superconductivity and non-fermi liquid at a quantum critical point in a metal. i. the γ model and its phase diagram at $T = 0$: The case $0 < \gamma < 1$, Phys. Rev. B **102**, 024524 (2020).

[2] Y.-M. Wu, A. Abanov, Y. Wang, and A. V. Chubukov, Interplay between superconductivity and non-fermi liquid at a quantum critical point in a metal. ii. the γ model at a finite T for $0 < \gamma < 1$, Phys. Rev. B **102**, 024525 (2020).

[3] Y.-M. Wu, A. Abanov, and A. V. Chubukov, Interplay between superconductivity and non-fermi liquid behavior at a quantum critical point in a metal. iii. the γ model and its phase diagram across $\gamma = 1$, Phys. Rev. B **102**, 094516 (2020).

[4] Y.-M. Wu, S.-S. Zhang, A. Abanov, and A. V. Chubukov, Interplay between superconductivity and non-fermi liquid at a quantum critical point in a metal. iv. the γ model and its phase diagram at $1 < \gamma < 2$, Phys. Rev. B **103**, 024522 (2021).

[5] Y.-M. Wu, S.-S. Zhang, A. Abanov, and A. V. Chubukov, Interplay between superconductivity and non-fermi liquid at a quantum critical point in a metal. v. the γ model and its phase diagram. the case $\gamma = 2$, Phys. Rev. B **103**, 184508 (2021).

[6] R. Combescot, Strong-coupling limit of eliashberg theory, Phys. Rev. B **51**, 11625 (1995).

[7] A. Karakozov, E. Maksimov, and A. Mikhailovsky, The investigation of eliashberg equations for superconductors with strong electron-phonon interaction, Solid State Commun. **79**, 329 (1991).

[8] F. Marsiglio and J. P. Carbotte, Gap function and density of states in the strong-coupling limit for an electron-boson system, Phys. Rev. B **43**, 5355 (1991) , for more recent results see F. Marsiglio and J. P. Carbotte, Electron-phonon superconductivity, in *The Physics of Conventional and Unconventional Superconductors*, edited by K. H. Bennemann and J. B. Ketterson (Springer-Verlag, Berlin, Heidelberg, 2008) and references therein; F. Marsiglio, Eliashberg theory: A short review, Ann. Phys. **417**, 168102 (2020).

[9] F. Marsiglio, M. Schossmann, and J. P. Carbotte, Iterative analytic continuation of the electron self-energy to the real axis, Phys. Rev. B **37**, 4965 (1988).

[10] Y.-M. Wu, A. Abanov, and A. V. Chubukov, Pairing in quantum critical systems: Transition temperature, pairing gap, and their ratio, Phys. Rev. B **99**, 014502 (2019).

[11] T.-H. Lee, A. Chubukov, H. Miao, and G. Kotliar, Pairing Mechanism in Hund's Metal Superconductors and the Universality of the Superconducting Gap to Critical Temperature Ratio, Phys. Rev. Lett. **121**, 187003 (2018).

[12] We note in passing that at $\gamma = \gamma_{cr}$, the two power-law solutions merge into a single $|\omega|^{\gamma/2}$, but at this point another solution $\Delta_\infty(\omega_m) \propto |\omega_m|^{\gamma/2} \log|\omega_m|$ emerges, as can be verified by using the identity $\int_{-\infty}^{\infty} dx |x|^{\gamma/2-1} \log|x|/|x-1|^\gamma = 0$. As a result, the low-frequency $\Delta_\infty(\omega_m) \propto |\omega_m|^{\gamma/2} \log|\omega_m|/\omega_*$ still contains a free parameter ω^* that allows one to match this low-frequency form with $\Delta_\infty(\omega_m) \propto 1/|\omega_m|^\gamma$ at high frequencies.

[13] The difference between the initial $\Delta_0(\omega_m)$ and the one, obtained by first computing $\Delta_0(\omega)$ using Pade approximants and then extending it back to the Matsubara axis by Cauchy relation, is better than 10^{-5} for $|z| \lesssim 5$, shown in Fig. 13.

[14] We note in passing that as long as $\gamma < 2$, the number of zeros in the upper half-plane is finite. Because each zero gives rise to 2π phase variation on the real axis (see paper IV), the phase winding of $\Delta_0(\omega)$ saturates at large ω, where both $\Delta_0'(\omega)$ and $\Delta_0''(\omega)$ become sign-preserving and scale as $1/\omega^\gamma$.

[15] A. V. Chubukov, A. Abanov, I. Esterlis, and S. A. Kivelson, Eliashberg theory of phonon-mediated superconductivity–when it is valid and how it breaks down, Ann. Phys. **417**, 168190 (2020).

[16] Y. Wang, A. Abanov, B. L. Altshuler, E. A. Yuzbashyan, and A. V. Chubukov, Superconductivity Near a Quantum-Critical Point: The Special Role of the First Matsubara Frequency, Phys. Rev. Lett. **117**, 157001 (2016).

[17] L. Yu, Bound state in superconductors with paramagnetic impurities, Acta Phys. Sin. **21**, 75 (1965).

[18] H. Shiba, Classical spins in superconductors, Prog. Theor. Phys. **40**, 435 (1968).

[19] A. Rusinov, Superconductivity near a paramagnetic impurity, ZETP Lett. **9**, 85 (1969).

[20] P. Nozières and C. T. De Dominicis, Singularities in the x-ray absorption and emission of metals. iii. one-body theory exact solution, Phys. Rev. **178**, 1097 (1969).

[21] D. V. Khveshchenko and P. W. Anderson, Fermi-edge singularities in x-ray spectra of strongly correlated fermions, Phys. Rev. B **61**, 1658 (2000).

[22] M. Hentschel and F. Guinea, Orthogonality catastrophe and kondo effect in graphene, Phys. Rev. B **76**, 115407 (2007).

[23] I. Affleck and A. W. Ludwig, The fermi edge singularity and boundary condition changing operators, J. Phys. A: Math. Gen. **27**, 5375 (1994).

[24] G. D. Mahan, Excitons in metals: Infinite hole mass, Phys. Rev. **163**, 612 (1967).

[25] P. W. Anderson, Infrared Catastrophe in Fermi Gases with Local Scattering Potentials, Phys. Rev. Lett. **18**, 1049 (1967).